On Parallel Hybrid-Electric Propulsion System for Unmanned Aerial Vehicles

Jane Yu-Chun Hung and Luis Felipe Gonzalez

Abstract

This paper presents a review of existing and current developments and the analysis of Hybrid-Electric Propulsion Systems (HEPS) for small fixed-wing Unmanned Aerial Vehicles (UAV). In recent years, development of UAV has become a significant growing segment of the global aviation industry. These vehicles are developed with the intention of operating in regions where the presence of onboard human pilots is either too risky or unnecessary. Their popularity with both the military and civilian sectors has seen the use of UAVs in a diverse range of applications, from reconnaissance and surveillance tasks for the military, to civilian uses such as aid relief and monitoring tasks. Efficient energy utilisation on an UAV is essential to its functioning, often to achieve the operational goals of range, endurance and other specific mission requirements. Due to the limitations of the space available and the mass budget on the UAV, it is often a delicate balance between the onboard energy available (i.e. fuel) and achieving the operational goals. One technology with potential in this area is with the use of HEPS.

In this paper, information on the state-of-art technology in this field of research is provided. A description and simulation of a parallel HEPS for a small fixed-wing UAV by incorporating an Ideal Operating Line (IOL) control strategy is described. Simulation models of the components in a HEPS were designed in the MATLAB Simulink environment. An IOL analysis of an UAV piston engine was used to determine the most efficient points of operation for this engine. The results show that an UAV equipped with this HEPS configuration described in this paper is capable of achieving a fuel saving of 6.5%, compared to the engine-only configuration.

NOMENCLATURE

ACM	Aircraft Control Module
BSFC	Brake specific fuel consumption
CBN	Charge Battery Now module
CMAC	Cerebellar model arithmetic computer
COTS	Commercially-off-the-shelf
CU	University of Colorado
CVT	Continuously variable transmission
DARPA	Defense Advanced Research Project Agency
DOF	Degree-of-freedom
EM	Electric motor
EO	Engine Operating module
ETC	Engine Throttle Command module
FC	Fuel-cell
FLC	Fuzzy logic controller
FPM	Flight Planner Module
GPS	Global Positioning System
HE	Hybrid-electric
HELIOS	Hybrid ELectric Integrated Optimized System; a CU project
HEPS	Hybrid electric propulsion system
HEUAV	Hybrid-electric UAV
hp	horsepower
ICE	Internal combustion engine
IOL	Ideal operating line
IPM	Intelilgent power management
Li-Po	Lithium-polymer battery
LUT	Look-Up Table
MAP	Manifold pressure
MAV	Micro air vehicle
NAV	Nano air vehicle

Jane Hung is with the Faculty of Built Environment and Engineering, Queensland University of Technology, Brisbane, QLD 4000 Australia. (E-mail: y.hung@qut.edu.au).

L. Felipe Gonzalez is with the Australian Research Centre for Aerospace Automation, Eagle Farm, QLD 4009, Australia; Smart Systems, Aerospace Avionics, Queensland University of Technology, Brisbane, QLD 4000 Australia. (E-mail: felipe.gonzalez@qut.edu.au).

OM	Operating Mode module
PD	Power Demand module
PI	Proportional and Integral controller
PID	Proportional, Integral and derivative controller
POA	Power Output Allocation module
RCR	Rate of Change of Ratio
RCRC	RCR Command module)
RPM	Revolutions per minutes
SOC	State-of-charge
SOLSTICE	Standalone-electric Optimized Lifting System, Transitional Internal Combustion Engine
TDC	Torque Difference Calculas
UAV	Unmanned aerial vehicle
UAVSM	UAV simulation model
XTE	Cross-track error

I. Introduction

An Unmanned Aerial Vehicle (UAV) is a "remotely piloted or self-piloted aircraft that can carry cameras, sensors, communications equipment or other payloads" [1]. UAVs have emerged as a viable platform to operate in regions where the presence of onboard human pilots is either too risky or unnecessary, in a diverse range of applications, from reconnaissance and surveillance tasks for the military, to civilian uses such as aid relief and monitoring tasks [2]. Their lower operation costs (as compared to manned aircraft and satellites) and availability in a great variety of sizes and capabilities have contributed towards the surging interest in UAVs from both the military and civilian sectors.

The focus of UAV applications has hitherto been predominantly in the military domain, but there has been increasing global interest in civilian and commercial UAV applications over the last decade, especially the use of small UAVs. Examples of these smaller cousins of the military UAVs, e.g. MQ-1 Predator or RQ-4 Global Hawk, include the Shadow, the Aerosonde, the Global Observer, the Bell Eagle Eye, the SkySeer, the ARCAA Flamingo UAV and the KillerBee 4 UAVs. The lower-cost factor of these small UAVs, much of which is due to the increase in the availability and quality of commercially off-the-shelf (COTS) components, and rapid increases in their capabilities as a result of technological advances, together present attractive incentives [3] for non-military and amateur UAV operators and developers, who are generally under more strict cost budgets when compared to their military counterparts.

Trade-offs between payload capability and aircraft endurance is always a problem that needs to be solved in the development and construction of UAVs, regardless of their size. As with all aircraft, there are mass and space limitations onboard UAVs for all onboard systems, including electronics, powerplant(s), fuel storage and payloads. However, these limitations are stricter for a small UAV due to their already smaller sizes.

The miniaturisation of avionics equipment and an increase in their capabilities have seen significant reductions in size, weight and power usage for small UAV components [4]. On the other hand, the use of COTS aeromodelling powerplants onboard a large proportion of emergent propeller-driven UAV platforms can be significantly disadvantageous in operational utility and energy efficiency compared to traditional aircraft powerplants [5]. While some UAV developers have successfully modified COTS aeromodel powerplants to achieve excellent efficiency, the utilisation of COTS components that are not sized ideally for the UAVs is still a common practice amongst civilian UAV developers, mostly due to cost issues. Consequently, the associated weight and space penalties contribute to limits on onboard fuel and/or energy resources (fuel, battery, etc.). This in turn brings about the problem of how to efficiently utilise the available energy resources onboard a small UAV.

One approach used in the research in the area of efficient energy usage onboard a small UAV is by developing and implementing alternative energy technology for use onboard the UAV. Examples of these include fuel cells, solar cells and hybrid propulsion systems. In this paper, the utilisation of a Hybrid-Electric Propulsion System onboard the UAV is investigated.

The rest of this paper is organised as follows: §II presents a brief background on HEPS, followed by §III with a description of the main Hybrid-Electric (HE) powertrain configurations that are most commonly in use today and an analysis of control methods for HEPS is given in §IV. §V presents a HEPS model which uses a Continuously Variable Transmission (CVT) and an Ideal Operating Line (IOL) control strategy, with the IOL analysis of the UAV Internal Combustion Engine (ICE) described in §VI, the component models of the HEPS powertrain in §VII and the HEPS controller in §VIII. A UAV Simulation Model is described in §IX and its integration and simulation results are presented in §X.

II. Hybrid-Electric Propulsion System

Traditionally, small civilian UAVs are mostly powered by ICE, but as they have a thermal efficiency of at most 40% [6] and, despite the high energy density of the liquid hydrocarbon fuels used by ICEs, with energy preservation issues on the rise, more efficient powerplant configurations have been sought.

A popular alternative powerplant is the Electric Motor (EM), which are capable of operating with an efficiency of close to 100% [7]. However, EM's high efficiency is negated by the necessary use of a power storage system which drives the EM in order to power the UAV. This power storage system, in most cases a battery, is often the largest component by weight in an UAV, representing a large weight penalty, as well as having a limited operating duration and relatively long period of time required to replenish its charge, resulting in a relatively short operating range and the need to charge frequently. Despite recent advances in power storage technology which have reduced the impact these drawbacks have had on the use of EM in civilian UAVs in the past, the sizes and relative inefficiencies of power storage systems still hold back the development of purely electrically powered UAV.

A way of overcoming the shortcomings of both powerplants is to integrate an ICE with an EM to form a Hybrid-Electric Propulsion System (HEPS). Hybrid propulsion technology has been an area of intense research, particularly by the automotive industry, and results have shown significant increases in fuel efficiency. On the other hand, the study of utilising hybrid propulsion in aircraft had only begun in recent years, and there has been little investigation on the various control methods for HE systems and their effects on aircraft, with previous efforts in this area being focused on the automotive industry.

III. HEPS Configurations

In a hybrid propulsion system, two or more power sources are combined together to increase the efficiency of the vehicle. There are various hybrid powertrain configurations currently in use, the most common being the following three configurations: series, parallel, and power-split. In the following descriptions, the focus is on system configurations that incorporate the gasoline ICE as the prime powerplant. However other engines - such as diesel, gas turbine, or fuel cells - are also being used on UAVs.

A. Series Configuration

In the series powertrain configuration, shown in Figure 1(a), the EM is the only means of providing power to the mechanical drive train. This means the ICE is able to operate in an optimum torque and speed range, regardless of the driving conditions, in the execution of its role as an auxiliary power unit to drive the EM to propel the aircraft, or the Generator to provide power to the energy storage system, or the Battery. The series configuration performs best for low-speed, high-torque applications such as in buses and other urban work vehicles. However, because the mechanical energy from the ICE is firstly converted to electrical energy in the Battery, then passed on to the EM, and lastly converted once again into mechanical energy to power the propeller, there exist large energy conversion losses between the mechanical and electrical systems. Thus the overall system efficiency is reduced [8]. Also, in the series configuration, although the ICE is typically smaller because it only has to meet average power demands, the EM and the Battery generally need to be sized larger to accommodate the peak power demands. This, combined with the Generator required in this configuration, results in a significant weight penalty, which is expensive onboard a UAV. Harmon [9] estimated that a series configuration for a small UAV can result in a 8%, or 2.5 lb (1.13kg), weight penalty for a 30-lb (13.61kg) UAV.

HEPS for UAVs have been considered by the Defense Advanced Research Project Agency (DARPA) in its Micro Air Vehicle (MAV) project in the form of a series HEPS that includes a diesel engine, generator, EM and battery pack [10]. Some details were provided in the report, however on smaller systems such as MAVs or Nano Air Vehicles (NAVs), in which both weight and size represent very strict constraints, a series HEPS is not suitable, due to the consequent weight penalty that usually results from its utilisation [11]. Research by Harmats and Weihs also concluded that series HEPS were not effective for use on UAVs due to large power losses [12].

The DA36 E-Star motor glider - developed by Siemens AG, Diamond Aircraft and EADS - is the world's first aircraft with a serial HEPS [13]. Recently made its debut at the Paris Air Show Le Bourget 2011, the two-seater motor glider is based on Diamond Aircraft's HK36 Super Dimona. Its propeller is powered by a 70kW EM, which is in turn powered by an ICE-generator combination. A battery system provides the power boost required during take-off and climb to the constant low output of 30kW from the ICE. According to the manufacturers, the DA-36 E-Star decreases fuel consumption and carbon emissions by 25% when compared to conventional aircraft.

B. Parallel Configuration

The parallel configuration, shown in Figure 1(b), enables the powering of the UAV using the ICE alone, the EM alone, or both depending on the operating conditions, as well as benefitting from redundancy, which is important in both civilian and military applications. Realisation of this configuration can be seen in various commercially available ground vehicles such as the Honda Insight, Civic and Accord hybrids [14]. Although this configuration can potentially suffer from an inability to operate the ICE in its most efficient region (it is directly coupled to the wheels in ground vehicles or the propeller shaft in aerial vehicles through a transmission, thus limiting the energy efficiency), integrating a Continuously Variable Transmission (CVT) in lieu of a conventional transmission will help to mitigate this potential problem. However, this introduces additional difficulty into the control strategy to schedule the torque from the individual or combined power sources for maximum efficiency [15, 16].

Work was carried out by Harmon *et al.* [17] in the conceptual design and simulation of a small UAV with a parallel HEPS. The design consists of an ICE sized for cruise speed and an EM and lithion-ion battery pack sized for endurance speed. A

rule-based controller based on the IOL concept was applied to this HEPS design to obtain simulation results, which showed significant energy savings when compared to a four-stroke gasoline-powered UAV (54% and 22% less energy use for a one-hour and three-hour intelligence, surveillance or reconnaissance mission respectively).

An example of a parallel HEPS implementation was developed for the Hyperion aircraft at the University of Colorado (CU) [18]. This gasoline-electric powerplant was originally developed as part of the Hybrid ELectric Integrated Optimized System (HELIOS) [19] project at CU and is now licensed by TIGON EnerTec, Inc, and was further expanded upon for the Hyperion as part of the Standalone-electric Optimized Lifting System, Transitional Internal Combustion Engine (SOLSTICE) project [20], also conducted at CU. This hybrid system combines power from an ICE and an EM to a single propeller shaft with a total power output of 4-hp (2.98kW), providing a combination of endurance and acoustic quietness, including high reliability, which cannot be provided by current purely electric UAVs. The electric-only mode enables UAV operations with a greatly reduced acoustic and infrared signature, which is advantageous when flying covert missions or around populated areas.

A German aircraft manufacturer, Flight Design, coupled a 40-hp (29.8kW) EM with a 115-hp (85.8kW) Rotax 914 aircraft ICE in a parallel HEPS configuration for a light-sport aircraft [21]. The EM provides approximately five minutes of boost power during take-off and climbing, which enables the down-sizing of the ICE from a 160-hp model to the more efficient 115-hp model. Additionally, the parallel configuration allows the pilot to prolong a glide with electric power in the event of engine failure, as well as utilising a form of regenerative braking by charging its battery pack through propeller wind-milling as the aircraft descends.

C. Power-Split Configuration

The power-split configuration, shown in Figure 1(c), has no direct connection between the various powerplants and the mechanical drive train. Instead, a planetary gear set is used to transfer the power generated by the ICE and/or EM to propel the UAV. This configuration is currently used on a number of vehicles today, including the Toyota Prius [22] and the Ford Hybrid Escape, but, to the knowledge of the authors, there is no implementation of a power-split HEPS on UAVs. The advantage of a power-split configuration over the other configurations is its comparative efficiency at reducing fuel usage and emissions, because it is able to combine the various power sources more efficiently. However, its very design introduces complexities in the cost and control strategies that are required for its operation.

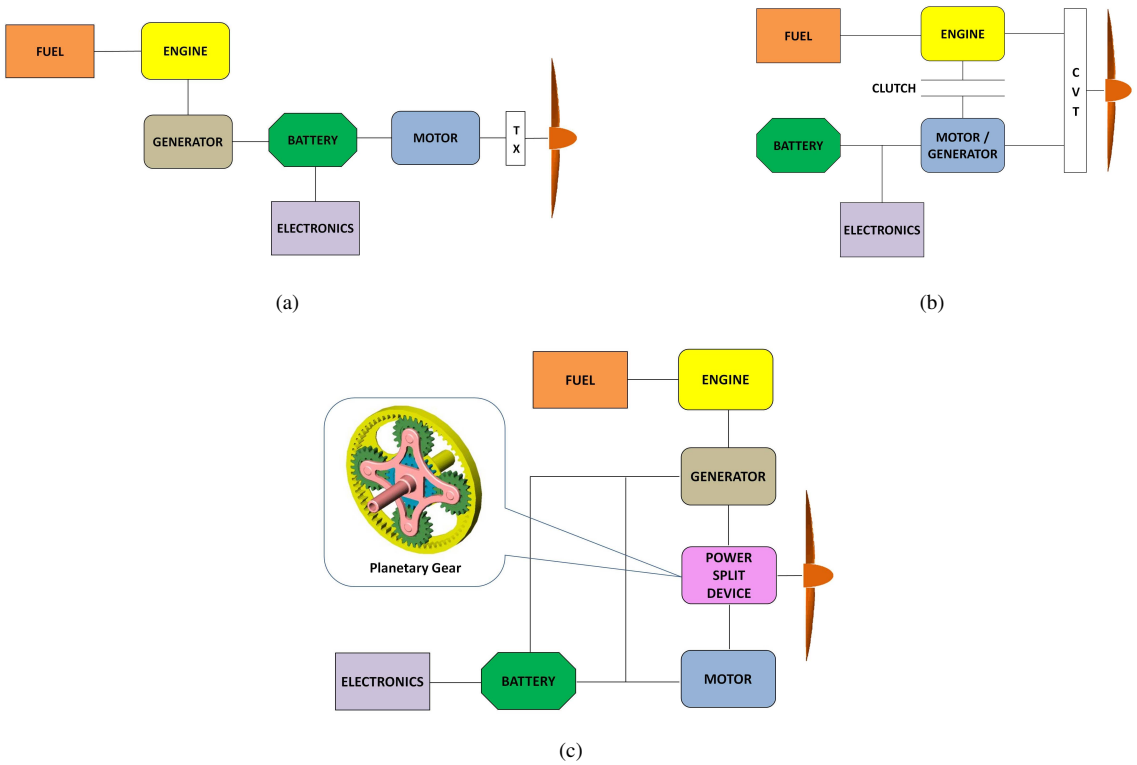

Fig. 1. HEPS configurations: (a) Series configuration; (b) Parallel configuration; and (c) Power-split configuration with planetary gear [23].

IV. HEPS Control Strategies

The HEPS controller is an integral component for a Hybrid-Electric UAV (HEUAV). It controls the main components of the HEPS - ICE, EM, Generator, Battery and CVT. The controller must be designed so that all the individual components operate

with each other to achieve the maximum efficiency. Different control strategies optimise a system using different methods. In this discussion, two main categories, intelligent controllers and rule-based controllers, will be described in §IV-A and §IV-B respectively.

A. Intelligent Controllers

Intense research has been conducted in the field of intelligent controllers. Several different types are currently used on hybrid automobiles today and these include fuzzy logic controllers and neural network controllers [24].

1) Fuzzy Logic Controllers: Fuzzy logic controllers (FLC) are basically rule-based controllers that use logical variables *between the values of 0 and 1* instead of just 0 or 1 [25]. Alptekin *et al.* [26] describe a FLC as appealing for its nonlinear modelling ability and robustness when faced with imprecise inputs. This characteristic makes FLC desirable for use in an aircraft, which is evident from proven implementation of FLC for applications such as autonomous flight control [27, 28]. Figure 2 shows two examples of FLC.

However, a major drawback stems from its simple method for determing solutions to problems. The use of rule sets to make decisions on nonlinear problems result in *exponential rule expansion*, where each input variable has a separate rule formed for each possible combination of input membership functions. This strategy works well for simple low-input systems, but even a small increase in the number of inputs can cause the rule sets to quickly increase to an unmanageable number. On the other hand, FLC has advantages when used for supervisory, task-oriented control. It can also permit the designer to design the control so that it will mimic his or her own preferences.

Many different FLC have been used in HEVs. In particular, Salman's controller focuses on the energy management for a charge-sustaining type of HEV [29]. Some research has been conducted in the area of power control strategies for the propulsion of UAVs, including the work by Karunarathne *et al.* [30] on a FLC for a fuel cell/battery hybrid system, although most UAV-related applications are still in the area of navigation and flight control.

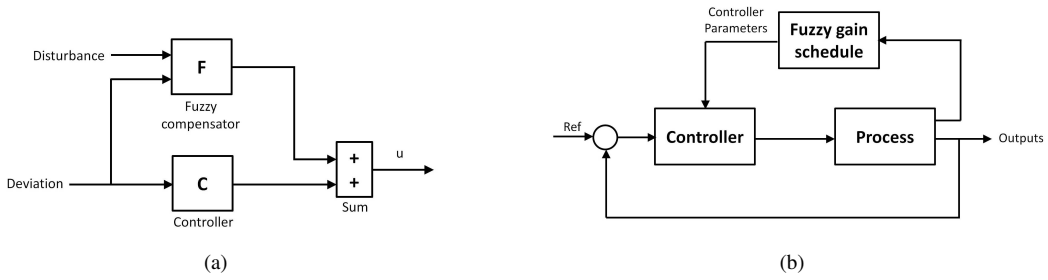

Fig. 2. Diagrams for (a) Feed-forward FLC and (b) Adaptive parameter FLC.

2) Neural Network Controllers: Neural network controllers are useful when the system is very difficult to model exactly. Such a controller attempts to mimic the human brain when modelling and controlling a system [24].

Similar to FLC, applications of neural network controllers in UAVs are mainly focused in the area of flight control, although some research has been conducted for management of UAV propulsion systems. An example of a neural network controller for HEUAV was the cerebellar model arithmetic computer (CMAC) neural network developed by Harmon [9]. This controller approximates an energy optimisation algorithm for the propulsion system which assigns relative importance between the use of gasoline, electricity and recharging. Simulation results show that a HEUAV with the CMAC controller uses 67.3% less energy than a two-stroke gasoline-powered UAV during an one-hour ISR mission and 37.8% in a three-hour ISR mission.

Karunarathne *et al.* [31] developed an adaptive neuro-fuzzy controller for fuel cell (FC)/battery driven unmanned electric aerial vehicles. The intelligent power management (IPM) strategy uses the battery state-of-charge (SOC) and load power variations in order to manage the FC system power output. This controller is compared with a static feed-forward controller to identify the power handling characteristics of the IPM system.

B. Rule-Based Controllers

Rule-based controllers have been used throughout history and are characteristically very reliable. Conceptually, a rule-based controller is the simplest type to understand and implement. Its simplicity and ease to design results in a relatively fast speed to make the calculations and decide on an action. Additionally, since the number of rules determines the complexity of the controller, it is only as complex as the designer makes it. In this aspect, a rule-based controller is similar to a fuzzy logic controller. However, unlike a fuzzy logic controller, rule count does not exponentially increase in a rule-based controller.

Much research has been conducted on rule-based controllers around the world, mostly tested or used in the automotive industry [32], but not many have been applied to HEUAVs. The IOL concept is one particular concept which would be suitable for a rule-based controller, and will be presented in more detail in §VI. This was used by Frank [33] and Francisco [15] to

optimise the fuel efficiency and lower emissions associated to ICE operation on hybrid-electric vehicles with a CVT in their systems, as well as to reduce powertrain part count while nost impacting cost. Cho [34] also used it in his research to optimise various vehicle emissions. This concept formed the basis of Harmon's CMAC neural network controller for HEUAVs [9]. A controller adopting this concept would operate the engine at the IOL in order to maximise the efficiency of the ICE. Details of this controller will be described in §VIII.

V. HEPS Model

As presented in §III and §IV, a Hybrid-Electric Propulsion System (HEPS) with a Continuously Variable Transmission (CVT), as shown in Figure 1(b) and utilising an Ideal Operating Line (IOL) control strategy has the potential to economise the energy efficiency on a small fixed-wing UAV. In order for these components to work in an organised manner, a controller is required. Its primary function will be to determine when and how each of the components of the HEPS will work in order to operate the ICE on the IOL, or a close approximation of this, while the UAV is in operation. For this reason, it will need to take into account the status and states of each of the HEPS components, in order to generate appropriate signals to operate the components accordingly. The IOL control strategy is used in the controller and a rule-based control strategy was selected because of its inherent simplicity.

With the inclusion of the IOL controller, the electro-mechanical components of the HEPS can be grouped as follows:

- Powertrain
  - Piston Engine (ICE)
  - Electric Motor (EM)
  - Generator
  - Battery
  - Transmission (CVT)
- IOL Controller

The development of a HEPS on an UAV can be accomplished in two stages:

1) Performing of an Ideal Operating Line (IOL) analysis on an active UAV ICE (§VI); and
2) Development and implementation of a HEPS simulation model (§VII).

Each of these HEPS components is implemented as a as MATLAB Simulink model. These models will form the complete UAV simulation model (UAVSM) of an HEUAV.

VI. Ideal Operating Line Analysis of an UAV ICE

The *Ideal Operating Line* (IOL), also known as the e-line, is a smooth line made up of all the points which represent the torque and speed combinations at which the fuel consumption is minimal on different power lines for steady-state conditions [35]. A powerplant operated on the IOL will, theoretically, enable the best performance while consuming the least amount of fuel possible.

Typically, finding the IOL for an engine requires an engine map, which is a plot of the performance of the engine to be analysed in terms of its RPM and torque output values, with the values represented as level contours of the corresponding brake specific fuel consumption (BSFC) values. Firstly, the lines of constant power output are plotted on the engine map. On each of these power lines, there is a point with the smallest fuel consumption. When all these points on all the power lines are connected together, the IOL is generated. Often these points do not form a smooth line, mainly due to the limited number of data points available in the engine map, as well as the very small fluctuations of fuel consumption in a rather large area. In order to obtain a workable IOL, a smooth line is fitted through these points and a polynomial function is created for this line.

The objective of this IOL analysis is to obtain the IOL for an UAV ICE. In this research, data for the Aerosonde ICE, as provided as part of the AeroSim Blockset package [36], was used. The UAV data - the power output and fuel flow at given values of engine RPM and manifold pressure (MAP) - for the ICE used are shown in Tables I and II.

A. ICE Torque Calculations

Using the power output values for the Aerosonde ICE (see Table I), the torque output can be calculated by:

$$Torque = \frac{Power \cdot 60}{2\pi \cdot RPM} \tag{1}$$

where $Power$ is in Watts (W) and the resulting $Torque$ is in Newton-metres (Nm). The resulting torque output values are shown in Table III.

RPM	MAP								
	60	**70**	**80**	**90**	**92**	**94**	**96**	**98**	**100**
1500	18.85	47.12	65.97	67.54	69.12	67.54	67.54	69.12	86.39
2100	59.38	98.96	127.55	149.54	151.74	160.54	178.13	200.12	224.31
2800	93.83	149.54	187.66	237.50	249.23	255.10	307.88	366.52	398.77
3500	109.96	161.27	245.57	307.88	326.20	351.86	421.50	591.14	531.45
4500	164.93	245.04	339.29	438.25	447.68	494.80	565.49	673.87	772.83
5100	181.58	245.67	389.87	496.69	528.73	571.46	662.25	822.47	993.37
5500	184.31	293.74	403.17	535.64	570.20	622.04	748.75	956.09	1059.80
6000	163.36	276.46	420.97	565.49	609.47	691.15	860.80	1131.00	1193.80
7000	124.62	249.23	417.83	586.43	645.07	762.36	996.93	1246.20	1429.40

TABLE I
TABLE OF POWER OUTPUT (W) AT GIVEN VALUES OF RPM AND MAP FOR THE AEROSONDE ICE

RPM	MAP								
	60	**70**	**80**	**90**	**92**	**94**	**96**	**98**	**100**
1500	31	32	46	53	55	57	65	73	82
2100	40	44	54	69	74	80	92	103	111
2800	50	63	69	92	95	98	126	145	153
3500	66	75	87	110	117	127	150	175	190
4500	83	98	115	143	148	162	191	232	246
5100	93	102	130	159	167	182	208	260	310
5500	100	118	137	169	178	190	232	287	313
6000	104	126	151	184	191	206	253	326	337
7000	123	144	174	210	217	244	321	400	408

TABLE II
TABLE OF FUEL FLOW (G/HR) AT GIVEN VALUES OF RPM AND MAP FOR THE AEROSONDE ICE

RPM	MAP								
	60	**70**	**80**	**90**	**92**	**94**	**96**	**98**	**100**
1500	0.12	0.30	0.42	0.43	0.44	0.43	0.43	0.44	0.55
2100	0.27	0.45	0.58	0.68	0.69	0.73	0.81	0.91	1.02
2800	0.32	0.51	0.64	0.81	0.85	0.87	1.05	1.25	1.36
3500	0.30	0.44	0.67	0.84	0.89	0.96	1.15	1.34	1.45
4500	0.35	0.52	0.72	0.93	0.95	1.05	1.20	1.43	1.64
5100	0.34	0.46	0.73	0.93	0.99	1.07	1.24	1.54	1.86
5500	0.32	0.51	0.70	0.93	0.99	1.08	1.30	1.66	1.84
6000	0.26	0.44	0.67	0.90	0.97	1.10	1.37	1.80	1.90
7000	0.17	0.34	0.57	0.80	0.88	1.04	1.36	1.70	1.95

TABLE III
TABLE OF TORQUE OUTPUT (NM) AT GIVEN VALUES OF RPM AND MAP FOR THE AEROSONDE ICE

B. ICE BSFC Calculations

On the other hand, the brake specific fuel consumption (BSFC) values can be calculated using the power output and fuel flow values (see Tables I and II) as follows:

$$BSFC = \frac{FuelFlow}{Power} \tag{2}$$

where $FuelFlow$ is in grams per hour (g/hr), $Power$ is in Watts (W) and the resulting $BSFC$ is in grams per Watt-hour (g/(W·hr)). The BSFC values are shown in Table IV.

RPM	MAP								
	60	**70**	**80**	**90**	**92**	**94**	**96**	**98**	**100**
1500	1.6446	0.6791	0.6973	0.7847	0.7957	0.8439	0.9624	1.0561	0.9492
2100	0.6736	0.4446	0.4234	0.4614	0.4877	0.5983	0.5165	0.5147	0.4949
2800	0.5329	0.4213	0.3677	0.3874	0.3812	0.3842	0.4093	0.3956	0.3837
3500	0.6002	0.4651	0.3543	0.3573	0.3587	0.3609	0.3559	0.3563	0.3575
4500	0.5032	0.3999	0.3389	0.3263	0.3306	0.3274	0.3378	0.3443	0.3183
5100	0.5122	0.4152	0.3334	0.3201	0.3159	0.3185	0.3141	0.3161	0.3121
5500	0.5426	0.4017	0.3398	0.3155	0.3122	0.3054	0.3098	0.3002	0.2953
6000	0.6366	0.4558	0.3587	0.3254	0.3134	0.2981	0.2939	0.2882	0.2823
7000	0.9870	0.5778	0.4164	0.3581	0.3364	0.3201	0.3220	0.3210	0.2854

TABLE IV
TABLE OF BSFC (G/W-HR) VALUES AT GIVEN VALUES OF RPM AND MAP FOR THE AEROSONDE ICE

C. Engine Map

In order to generate the engine map from the torque and BSFC data, a contour plot was utilised. Each of the lines on the plot, called contours, are formed by joining the operating points that have the same BSFC value. Because there is equal spacing of BSFC values from one contour to the next, a region of dense contours represents the presence of a "steep" slope, whereas a region of widely spaced contours illustrates a "gentle" slope. In other words, an engine map is similar to a relief map, but instead of showing contours of equal altitude like a relief map does, an engine map shows contours of equal BSFC. In this case, the computation of these contours involved much estimation by inter- and extrapolation, since the available data are fairly limited in their descriptions of these engine characteristics.

Tables III and IV, calculated from Tables I and II, provide some data for the formulation of the contour plot, but in order to generate one with more details, more data values were required. These new values of power and fuel flow were obtained by performing open throttle calculations, i.e. setting the throttle value to 1 (full throttle) and varying the static pressures (to simulate the changing in altitude) and the RPM. Using Equations 1 and 2, the corresponding values for torque and BSFC were calculated. The fuel map was generated from these data values and is shown in Figure 3(a).

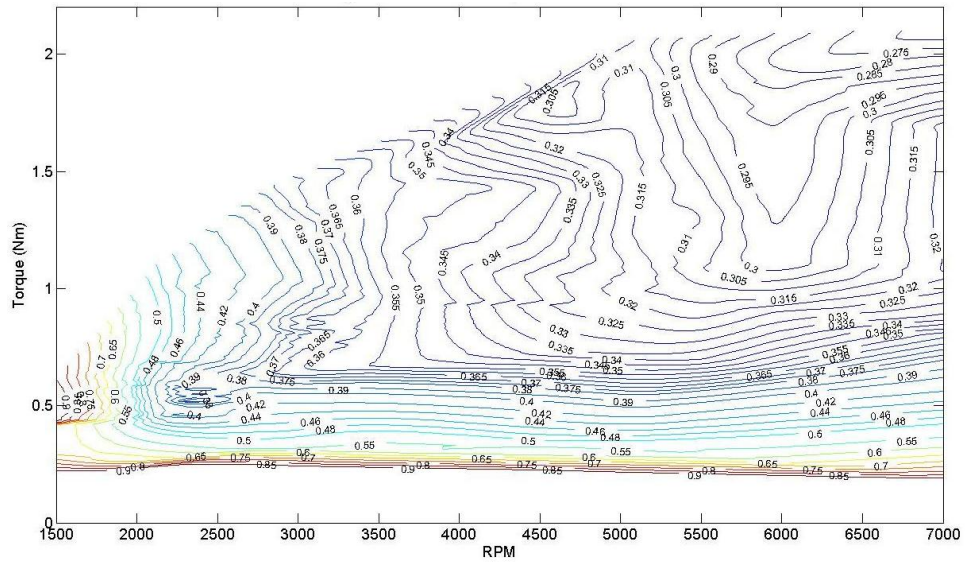

(a)

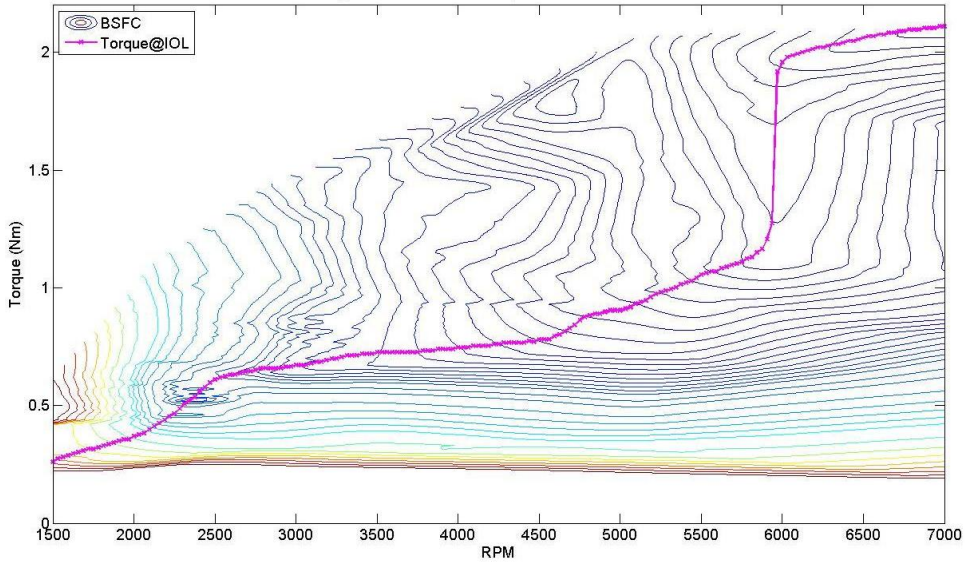

(b)

Fig. 3. Engine fuel map: (a) With BSFC contours using ICE data and open throttle calculations; and (b) With the IOL (magenta).

D. Determining the IOL

The next step was determining the IOL. In order to do this, the power contours are required. These power contours were then superimposed onto the engine map. On each of the power contours, the point with the smallest BSFC value was identified, and connecting the point for all the power contours on the plot gives the IOL, illustrated in Figure 3(b). For each of these points on the IOL, the corresponding BSFC values were obtained from this graph. These, along with the torque values, form the basis of operating the ICE on the IOL.

Figure 4(a) shows the power and torque values for each point on the IOL, while Figure 4(b) illustrates the BSFC and fuel flow values. The power and fuel flow values were obtained from the torque and BSFC values using Equations 1 and 2. The next and final step of the IOL analysis was to determine the corresponding MAP values to these torque and BSFC values. The power and fuel flow look-up tables (Tables I and II) were used to do this. The results are shown in Figure 4(c).

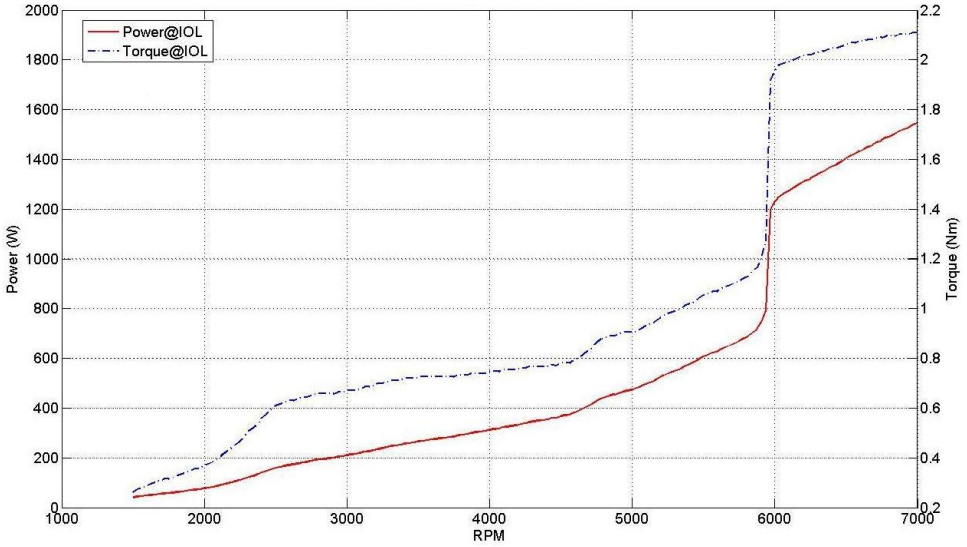

(a)

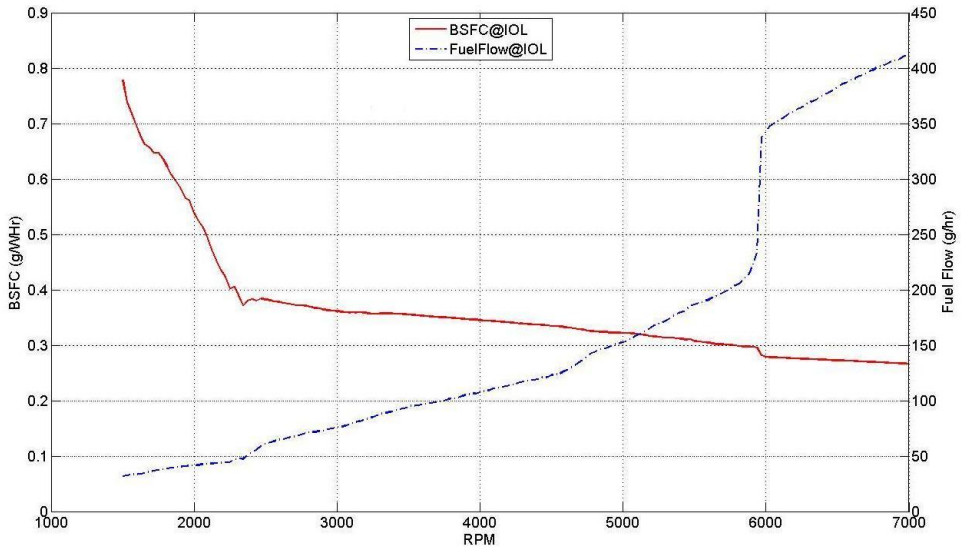

(b)

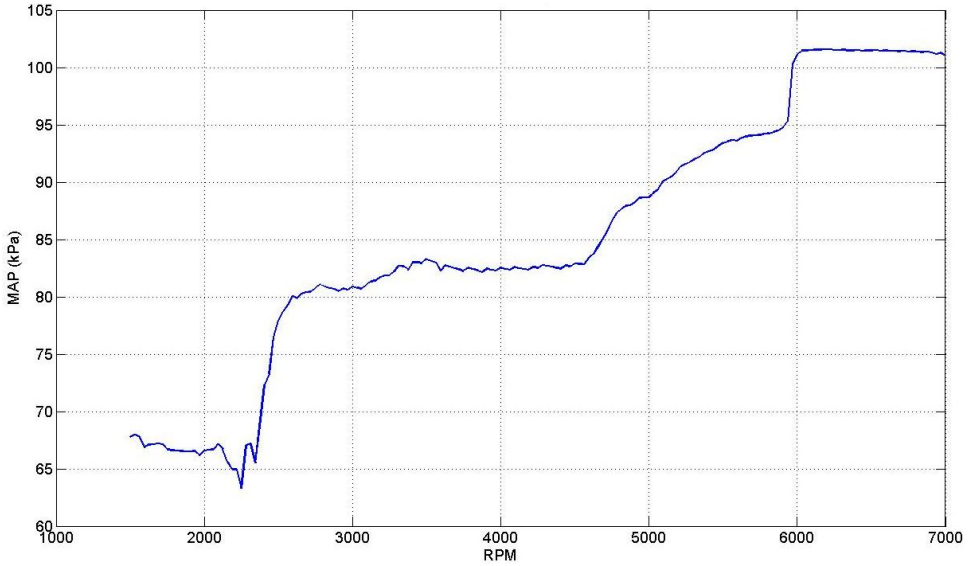

(c)

Fig. 4. Data values for the IOL: (a) Power (red) and torque (blue); (b) BSFC (red) and fuel flow (blue); and (c) MAP.

VII. HEPS Powertrain

Computer simulations are commonly used nowadays as actual flight tests are often extremely time-consuming as well as cost-prohibitive. A UAV Simulation Model (UAVSM) was developed to simulate the control and operation of a mission of an UAV equipped with a HEPS.

The MATLAB Simulink environment and the AeroSim Blockset were chosen for the UAVSM implementation. The AeroSim Blockset [36] is a commonly used aircraft simulation and analysis package in the aerospace industry, providing a comprehensive set of tools for development of non-linear 6-degrees-of-freedom (6DOF) aircraft models. It also offers a detailed set of parameters and a model of an Aerosonde, a small real-world fixed-wing UAV, which can be incorporated into the aircraft model to simulate the UAV in flight. The UAV block consists of a detailed model of the inner workings of the UAV, which consists of Aerodynamic, Propulsion, Atmosphere, Aircraft Inertia, Acceleration and Moments, Equations of Motion and Earth models.

The components that required modelling are:

- Electric Motor (EM);
- Generator;
- Battery;
- Transmission (CVT);
- Powertrain Output Allocation (POA) module; and
- Charge Battery Now (CBN) module.

Of the HEPS Powertrain components, the Piston Engine (ICE) and Fuel components are already present in the UAVSM, and they remained as they were to maintain the integrity of already working components.

A. Piston Engine Model

The Piston Engine (ICE) is the primary source of propulsion in the HEPS. The goal of the HEPS is to operate the ICE on the Ideal Operating Line (IOL) as determined in §VI. The preset configuration of the Piston Engine block from the AeroSim Blockset [36] was used in this research. The modelling of the simple ICE is achieved using two-dimensional Look-Up Tables (LUTs) of engine parameters. Given a set of RPM and manifold pressure (MAP) values, the corresponding values for fuel flow and engine power at sea level are determined and these are used in computations of other ICE outputs. In this research, the engine parameters of an Aerosonde engine were used.

B. Electric Motor Model

The function of the Electric Motor (EM) within the HEPS is two-fold. It acts as a supplementary powerplant to the ICE when required, or as the sole powerplant when the UAV is operating in Motor-only mode. This particular mode is most likely for the performance of a particular task, i.e. data collection or aerial imaging.

The EM model is created and simulated by approximating a Look-Up Table (LUT) and uses a pre-existing set of input-output values and interpolation and/or extrapolation methods to associate a given input to the appropriate output. This method is suitable in the modelling of EMs as the outputs (mainly torque and power) are usually controlled by and has a direct relationship with the input current.

The EM model will only output Motor Power and Torque values and draw current from the Battery if it is activated (i.e. when $MotorEnable = 1$), and when the Battery has adequate SOC and can provide enough voltage.

Here the EM model is implemented using data from a Plettenberg HP220/25 EM with constant 18V input to construct the LUTs. This particular model of EM was selected because it is capable of producing the power and torque required by the Aerosonde UAV in level flight. However, switching to another EM model will not be complicated, if data is available for a different EM.

C. Generator Model

Physically, the Generator and the EM are the same machine. But functionally, the Generator module is assumed to be the "reverse" of EM. Its only function is to provide the battery with charging current when there is extra torque available in the propulsion system, i.e. from the ICE.

As with the EM model, the Generator model will not output any values unless it is activated, i.e. $GeneratorEnable = 1$. Note that it is physically impossible to activate both the EM and the Generator at the same time. If EM is activated, the Generator needs to be deactivated, and vice versa. This will need to be taken into account by the HEPS control strategy to ensure correct functioning of these two modules.

D. Battery Model

The main function of the Battery model is to provide the required current and voltage to the onboard avionics and also to the EM when its activation is required. Additionally, the Battery needs to switch to charging when excess torque is available in the system, i.e. from the ICE. The discharging characteristics for a lithium-polymer (Li-Po) battery can be modelled by the following equation [37]:

$$E = E_0 - K \cdot \frac{Q}{Q - i \cdot t} + Ae^{-B \cdot i \cdot t} \tag{3}$$

where

$$\begin{aligned} E &= \text{battery output voltage (V)} \\ E_0 &= \text{battery constant voltage (V)} \\ K &= \text{polarity voltage (V)} \\ Q &= \text{maximum battery capacity} \\ A &= \text{exponential voltage coefficient} \\ B &= \text{exponential capacity coefficient (Ah}^{-1}\text{)} \\ i &= \text{battery current (A)} \\ t &= \text{time (s)} \end{aligned}$$

The charging characteristics of the Battery modes are considered to follow Equation 3 as well, although with a negative current to indicate charging instead of discharging.

Another important characteristic of a Battery is its State-of-Charge (SOC), which is approximated by [22]:

$$SOC = 100 \left(1 - \frac{\int_0^t i \cdot t}{Q} \right) \tag{4}$$

Here, the *Battery Subsystem* module is implemented using the data of two Air Thunder 5000mAh 6-cell Lithium-polymer (Li-Po) Battery Packs [38] in series to obtain the required output voltage for the EM. These particular batteries were selected because of their ability to meet the eletrical requirements (voltage and current) to power the Plettenberg EM, as well as their availability as a COTS commodity. The discharge curves for different amount of current drawn from the Battery are shown in Figure 5. These discharge curves are fitted to (3) in order to establish the coefficients K, Q, A and B. These coefficients are determined using an interpolation function.

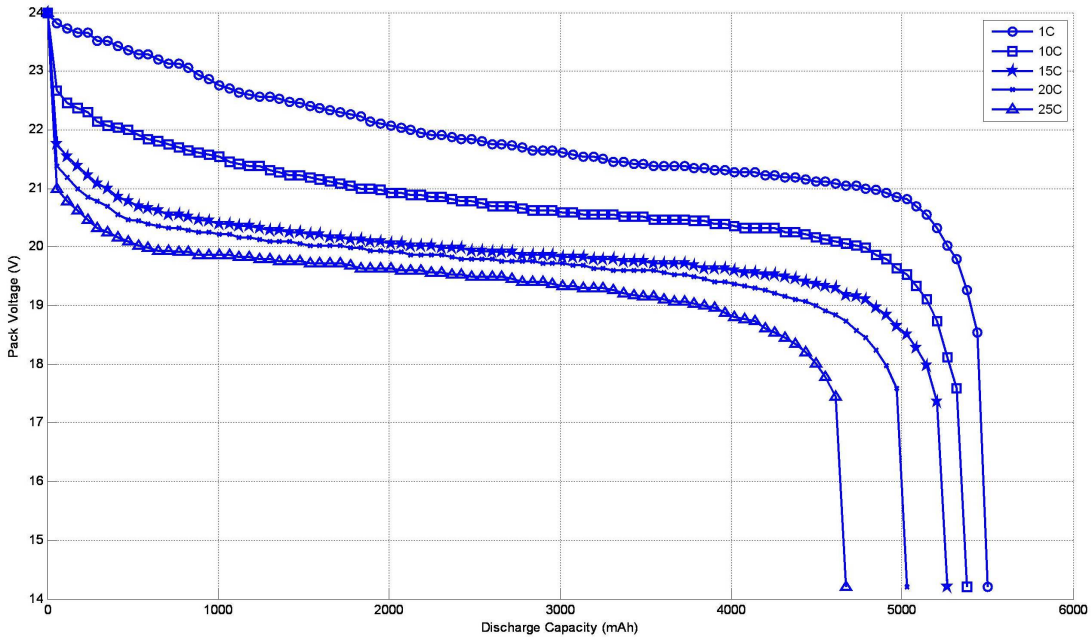

Fig. 5. Battery discharge curves.

E. CVT Dynamics Model

The type of transmission implemented in the HEPS is a Continuously Variable Transmission (CVT). In a conventional gearbox, output torque and speed of the engine are transmitted in discrete ratios, and the action of changing from one gear to another interrupts the power frow through the powertrain during the acceleration. One way of overcoming this intermittent behaviour is with the use of a CVT, which has the capability to transmit engine torque and speed in an undefined number of ratios [39]. This enables the output of a smooth, rapid and stepless response to the demand of the controller. Additionally, a CVT allows the engine speed to be operated independently of the vehicle speed (wheel speed for a ground vehicle or propeller speed for an aircraft, for example), therefore the engine can, in theory, be operated in its most fuel efficient operating point, with the help of a suitable controller strategy to control the CVT operations. The CVT's potential of reducing fuel consumption and lower the output of exhaust emissions has been confirmed various research projects [40, 41].

The dynamics of the CVT can be modelled by the following expression derived from a simplified powertrain with a CVT [15, 33]:

$$\dot{\omega}_{prop} = \frac{T_{prop} + rT_p - \dot{r}\omega_{eng}I_p}{I_{prop} + r^2 I_p} \tag{5}$$

where

$$\begin{aligned}
\omega_{eng} &= \text{rotational velocity of the engine (rad/s)} \\
\omega_{prop} &= \text{rotational velocity of the propeller (rad/s)} \\
\dot{\omega}_{prop} &= \text{rate of change of the propeller rotational velocity (rad/s}^2\text{)} \\
T_{prop} &= \text{propeller torque (Nm)} \\
T_p &= \text{powertrain torque (Nm)} \\
I_p &= \text{total powertrain (ICE + EM) torque} \\
I_{prop} &= \text{total propeller inertia} \\
r &= \frac{\omega_{eng}}{\omega_{prop}}\text{; transmission ratio} \\
\dot{r} &= \text{rate of change of ratio (RCR)}
\end{aligned}$$

The output of this equation is the rate of change of the propeller speed, $\dot{\omega}_{prop}$ using the other parameters, from which the propeller speed ω_{prop} can be determined with a simple integration process. To prevent overlarge values of $\dot{\omega}_{prop}$ from appearing, a saturation function was used to limit the $\dot{\omega}_{prop}$ output.

F. Charge Battery Now (CBN) Module

A module that is included inside the *Powertrain* block is the Charge Battery Now (CBN) module. This module monitors the charging and discharging of the Battery as well as estimates the time remaining before the UAV is required to go into "Motor Only" mode. Because this mode is an important part of the mission, and since the EM requires adequate Battery SOC and voltage in order to operate, therefore it is important that the Battery is maintained at a very high level of SOC as the UAV approaches the "Motor Only" mode. This is achieved by estimating, at any one time, the amount of time it requires to charge the Battery back to 100%.

G. Powertrain Output Allocation (POA) Module

The combined power and torque outputs of the Powertrain components - namely the ICE, EM and Generator - are passed to and used in the CVT Dynamics component as well as the subsequent components of the Aircraft block for further computations in the simulation of an HEUAV in flight. However, a slight difference between the values to be passed to each of these destination in the form of a *Rate of Change of Ratio Compensation Torque*, or RCR Torque (see §VIII-E for further description), is required to be taken into consideration. This term is the result of the shifting of the CVT whilst in operation and needs to be compensated by the torque output of either EM or Generator. Therefore the combined Powertrain torque output into the CVT Dynamics component requires the corresponding compensation term to be included. On the other hand, the compensation torque is not required in the output to the subsequent AeroSim components. The Powertrain Output Allocation (POA) module was implemented to allow for this distinction.

VIII. HEPS IOL Controller

The implementation of a HEPS on an UAV requires a controller which manages the operation of each of the system components – ICE, EM, Generator and Battery – so that operation on the IOL, or a close approximation of this, can be achieved while the UAV is in operation.

The basic control loop of this implementation of the IOL Controller when in Hybrid mode is shown in Figure 6.

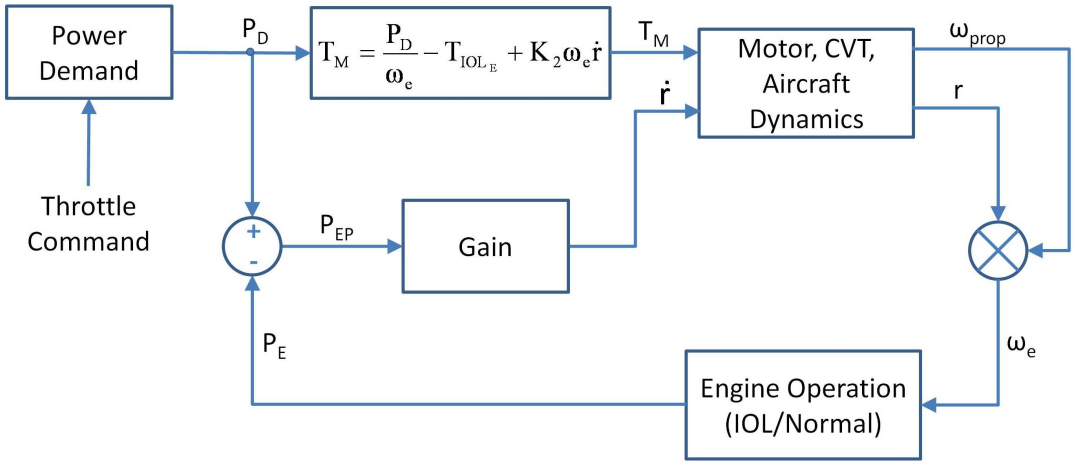

Fig. 6. The basic control loop of the IOL Controller.

The concept behind this control loop is that the Aircraft Control Module in the UAVSM demands a specific throttle opening, which is converted to a power demand measurement and from this, the desired torque that needs to be matched or closely approximated by the HEPS is computed. However, the Engine should be operating on the IOL, thus producing a torque value which is often different to the desired torque. The difference between the torque values is provided by either the EM or the Generator - the EM provides extra torque required if IOL torque is less than desired torque, otherwise the Generator uses the excess torque to charge the Battery.

On the other hand, this torque difference is multiplied by the engine speed to determine the power error. This power error is used to determine the Rate of Change of Ratio (RCR) value within a preset limit, which determines the amount of shifting that is required of the CVT.

The components of the IOL controller are as follows:

- Operating Mode module;
- Power Demand module;
- Engine Operation module;
- Engine Throttle Command module;
- Rate of Change of Ratio Command module; and
- Torque Difference Calculation module.

which are integrated together to form the IOL Controller as shown in Figure 7.

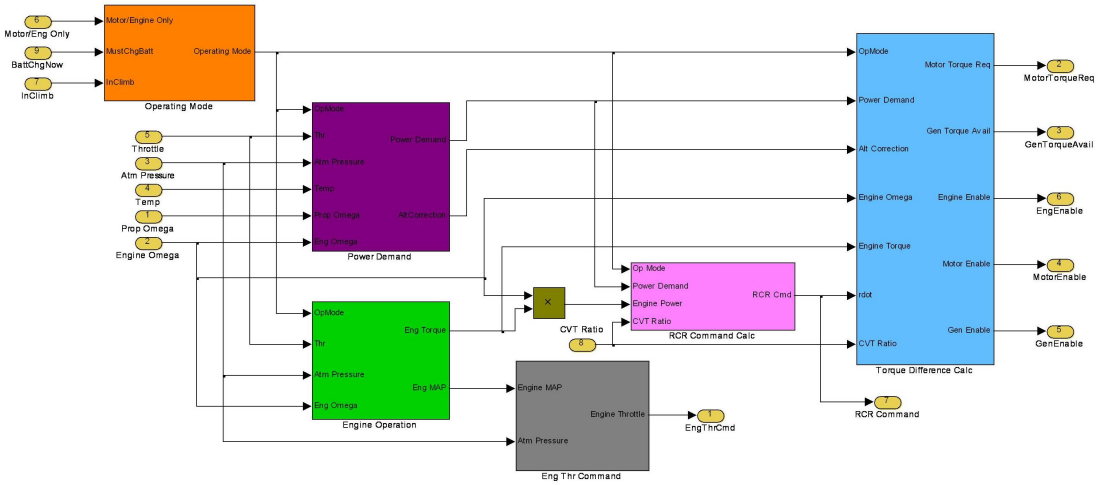

Fig. 7. Inside the *IOL Controller* block.

The details of each of these components and its functions are described in the following sub-sections.

A. Operating Mode (OM) Module

The Operating Mode (OM) module determines the mode in which the HEPS is currently operating in. These modes can be one of the following: Hybrid Normal mode, Motor Only mode, Hybrid Charging mode, Engine Only mode, and Hybrid Climbing mode.

The conditions for the switching of the operating modes are summarised in Table V. The default operating mode is the *Hybrid Normal* mode, during which the ICE is operating on the IOL, with the EM or Generator supplementing when a sudden increase or decrease in the power demand occurs. If the "Motor Only" signal has been detected, which can only occur at pre-planned, specified leg(s) of the mission, the operating mode switches over to *Motor Only* mode, and only the EM is powering the UAV to maintain its operation. If the "Must Charge Battery" signal, as generated by the CBN module in the Powertrain (see §VII-F), is detected, the *Hybrid Charging* mode is triggered if the aircraft is not required to climb to a higher altitude (i.e. $InClimb = 0$), during which the ICE is operated at an Engine speed to provide excess torque to power the Generator and thus charge the Battery. Otherwise, the *Engine Only* mode is engaged in order to preserve fuel consumption since charging the Battery requires the ICE to run at regions with higher fuel consumptions. If charging of the Battery is not required and a higher altitude is desired (i.e. $InClimb = 1$), the *Hybrid Climbing* mode is engaged and the EM is activated to provide extra torque to assist the ICE in the climb. Lastly, if the "Engine Only" signal has been detected, which only occurs at pre-planned, specific leg(s) of the mission, the HEPS would operate in the *Engine Only* mode.

Operating Mode	Condition
Hybrid Normal	- Default operating mode - When Battery SOC is at least 15%
Motor Only	Only when the *Motor Only* signal is detected
Hybrid Charging	When *MustChgBatt* signal is detected AND no climbing is required
Engine Only	When the *Engine Only* signal is detected OR When *MustChgBatt* AND *InClimb* signals are detected simultaneously
Hybrid Climbing	When *InClimb* signal is detected AND no charging of Battery is required

TABLE V
SWITCHING CONDITIONS OF OPERATING MODES.

B. Power Demand (PD) Module

The Power Demand (PD) module is the *beginning* of the IOL Controller control loop. PD takes the throttle input from the ACM block outside the UAV block, which was determined using a PID controller on the aircraft altitude error, and uses it to determine the amount of power required to be generated by the Powertrain if just the ICE was powering the UAV. In the ICE-only configuration of the UAV, this throttle input is fed directly to the *Piston Engine* block, which uses this, along with other parameters, to determine the power, torque and fuel consumption and their related outputs from the ICE. These outputs are the amounts required for the UAV to operate as desired. Based on this concept, PD uses parts of this *Piston Engine* block, namely the MAP and Power LUT blocks, to determine the power required to keep the UAV operating as desired. The functionality of PD in the various operating modes is summarised in Table VI.

Operating Mode	Process
Hybrid Normal Motor Only Engine Only	Converts Throttle command from ACM into the Power Demand, using current Propeller speed at the current altitude
Hybrid Charging	Converts Throttle command from ACM into the Power Demand, using current Propeller speed at the current altitude and add the *Generator Charging Torque*
Hybrid Climbig	Converts Throttle command from ACM into the Power Demand, using current Propeller speed at the current altitude and subtract the *Motor Climbing Torque*

TABLE VI
FUNCTIONALITY OF THE *Power Demand* MODULE.

Note that in the *Piston Engine* block, the effect of altitude on the Engine outputs has been taken into account. This is required in calculations for all outputs related to engine power. Therefore this altitude correction factor is necessary in later power- and torque-related calculations.

In the *Piston Engine* block, the torque is derived from the engine power output following the relationship described in Equation 6.

$$Power_{@alt} = Power \cdot altCorrection \tag{6}$$

Also:

$$Torque_{@alt} = \frac{Power_{@alt}}{\omega} \tag{7}$$

Substituting Equation 6 into Equation 7 gives:

$$Torque_{@alt} = \frac{Power}{\omega} \cdot altCorrection \tag{8}$$

And lastly, substituting in the definition of Torque into Equation 9:

$$Torque_{@alt} = Torque \cdot altCorrection \tag{9}$$

In the PM module, this altitude correction factor, $altCorrection$, is calculated, but not yet applied to the power value required. This factor is passed on to the Torque Difference Calculation module for further processing.

C. Engine Operation (EO) Module

A critical step in the IOL control loop is to determine the ICE outputs, in particularly the torque output. During a mission, an ICE can operate either by itself, in which the ICE operates in the normal manner (i.e. not constrained to the IOL), or in conjunction with the EM or Generator, in which the ICE would be operating on the IOL. For this reason, a good approximation of the ICE outputs in each of these operating modes is required in order to proceed to the remainder of the processes in the IOL control loop. The Engine Operation (EO) module was designed and implemented to perform this approximation of ICE outputs.

The main components in the EO module are the LUTs to determine the torque and manifold pressure (MAP) values for normal ICE and IOL modes of operation. In each time step in the simulation, these outputs are obtained from the current engine speed and, in the case of normal ICE operation, the MAP using atmospheric conditions. These outputs are then passed through a MATLAB function, which takes into consideration the current operating mode (see §VIII-A) and determines the appropriate torque and MAP values to be used in subsequent calculations.

D. Engine Throttle Command (ETC) Module

The Engine Throttle Command (ETC) module computes the Engine throttle required to operate the Engine on or close to the IOL. This module uses Equation 10, with the MAP calculated by EO module for IOL operation and the static pressure at the current altitude, to calculate the throttle command.

$$thr = \frac{MAP - MAP_{min}}{\frac{p}{1000} - MAP_{min}} \tag{10}$$

The output of ETC, the Throttle Command, is passed to the *Powertrain* subsystem, to be used as input into the *Piston Engine* block.

E. Rate of Change of Ratio Command (RCRC) Module

The Rate of Change of Ratio Command (RCRC) module determines the value for the rate of change of ratio (RCR), which is an important parameter in controlling the CVT in order for the HEPS to operate in the desired manner. The computation of the RCR command is dependent on the operating mode from OM module (see §VIII-A).

When the HEPS is operating in a Hybrid mode, the RCR is simply computed using the power error and a gain in the following manner:

$$\begin{aligned} \dot{r}_{cmd} &= Gain \cdot PowerError \\ &= Gain \cdot (PowerDemand - EngPower) \end{aligned} \tag{11}$$

(12)

where $PowerDemand$ is the output from the PD module (see §VIII-B) and $EngPower$ from the EO module (see §VIII-C). The $Gain$ is taken as $1/2000$ in this research. The resulting *RCR Command* value is then limited between -0.1 and 0.1 so that the CVT is not subjected to a large change in its ratio.

On the other hand, when the HEPS is operating in either of the *Motor Only* or *Engine Only* modes, it is desired that the Engine is being operated at the same speed as the Propeller, i.e. $\omega_{eng} = \omega_{prop}$ or $r = 1$. Therefore, when the *Motor Only* or *Engine Only* signal is first detected, the *RCR Command* is set at a value which would increase or decrease the CVT ratio to 1 in 10 time steps. In this research, the simulations are performed with a fixed step size of 0.1 second. This means the CVT reaches a ratio of 1 one second after the *Motor Only* or *Engine Only* signal has been detected. After the 10 time steps, the *RCR Command* is set at zero so that the CVT can maintain a ratio of 1 to keep the Engine operating at the same speed as the Propeller.

The output of the RCRC module is used mainly in the *Subsystem_CVTDynamics* to control the CVT ratio, but it is also used in the *RCR Compensation Torque* calculations in the *Torque Difference Calculation* module.

F. Torque Difference Calculation (TDC) Module

The Torque Difference Calculation (TDC) module not only computes difference between the desired torque and the IOL torque, it also uses this and other inputs to determine the enable/disable signal to the Engine, EM and Generator modules, as well as to compute the amount of torque available to the Generator or required from the EM.

The use of CVT in the system introduces a torque term, or RCR Torque, which needs to be compensated by the powertrain. This term is given by Equation 13, which is extracted from Equation 5:

$$RCRTComp = \dot{r}\,\omega_{eng} I_p \tag{13}$$

This term is negated by the EM, the torque output of which can be expressed as follows:

$$T_M = TorqueDiff + k_2 \omega_{eng} \dot{r} \tag{14}$$

where k_2 is a constant.

Substituting Equation 14 into Equation 5 gives:

$$\begin{aligned} \dot{\omega}_{prop} &= \frac{r\left(T_E + TorqueDiff + k_2\omega_{eng}\dot{r}\right) - \dot{r}\left(J_E + J_M\right)\cdot\omega_{eng} - T_{prop}}{J_{prop} + r^2\left(J_E + J_M\right)} \\ &= \frac{r\left(T_E + TorqueDiff\right) + rk_2\omega_{eng}\dot{r} - \dot{r}\left(J_E + J_M\right)\cdot\omega_{eng} - T_{prop}}{J_{prop} + r^2\left(J_E + J_M\right)} \end{aligned}$$

For the EM or Generator to negate the effect of the $-\dot{r}\left(J_E + J_M\right)\cdot\omega_{eng}$ term, the following evaluation of k_2 can be assumed:

$$\begin{aligned} rk_2\omega_{eng}\dot{r} &= \dot{r}\left(J_E + J_M\right)\cdot\omega_{eng} \\ k_2 &= \frac{J_E + J_M}{r} \end{aligned}$$

All the TDC outputs are passed to the *Powertrain* block to their respective component models.

IX. UAV Simulation Model

The complete UAVSM, is shown in Figure 8. The Aircraft Control Module (ACM) (§IX-B) and Flight Planner Module (FPM) (§IX-A) were developed and added to the Aerosonde UAV block to simulate unmanned operations, while most elements of the HEPS were described in §VII and §VIII. The ACM and FPM blocks are shown in red in Figure 8.

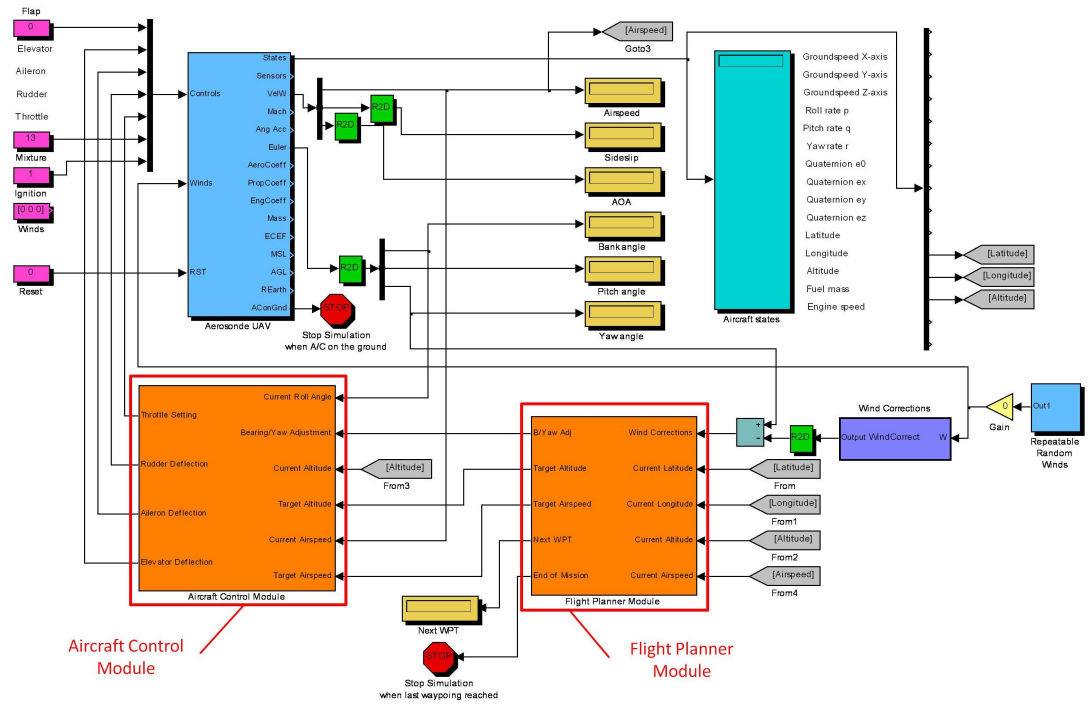

Fig. 8. The UAV Simulation Model, showing the Aerosonde UAV block and the ACM and FPM blocks.

A. *Flight Planner Module (FPM)*

The Flight Planner Module (FPM), detailed in Figure 9, enables the testing of the HEPS for different flight missions. The main component inside the FPM is a MATLAB function, *NavigateWaypoints*, which carries out the task of waypoint navigation. Given a set of waypoints in their GPS coordinates (latitudes, longitudes and altitudes), *NavigateWaypoints* calculates the necessary bearing/yaw adjustment the aircraft is required to make in order for it to fly from its current position to the next waypoint.

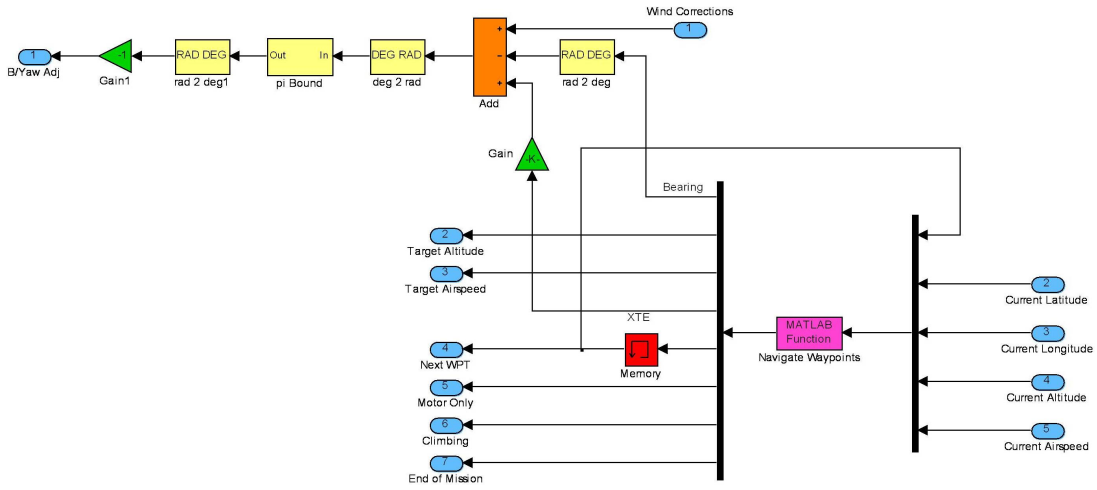

Fig. 9. Flight Planner Module.

The *NavigateWaypoints* function uses a basic navigational algorithm based on the great-circle navigation method [**?**], which calculates the great circle track, or the shortest distance following the curvature of the Earth, and the bearing between the two points, as shown in Figure 10(a). Thus, the aircraft flies through the series of waypoints by flying a sequence of direct, curved paths from one waypoint to the next. Using spherical trigonometry, the range D and bearing B_T to the target are given by [**?**]:

$$D = R_G \cos^{-1}\left(\sin\phi \sin\phi_t + \cos\phi \cos\phi_t \cos(\lambda - \lambda_t)\right) \quad (15)$$

$$B_T = \sin^{-1}\left\{ \frac{\cos\phi_t}{\sin\left(\frac{D}{R_G}\right)} \sin(\lambda - \lambda_t) \right\} \quad (16)$$

$$R_G = \sqrt{R_M \cdot R_P} \quad (17)$$

where R_G is the Gaussian radius of curvature at the current location, R_M and R_P are the meridian and prime radii, respectively, at the current location, (ϕ, λ) are the latitude and longitude at the currently location, and (ϕ_t, λ_t) are the latitude and longitude at the target point. This calculated distance to target is in fact the *distance-to-go* to the target, since the aircraft position is constantly changing.

Another factor that needs to be considered for the aircraft to follow the flight path set by the series of waypoints is the cross track error, or XTE, which is calculated by [**?**]:

$$XTE = DTR \cdot \sin(\theta_{TE}) \quad (18)$$

where DTR is the *track distance*, or the distance from the current location to the next waypoint, and θ_{TE} is the angle of track error. This relationship is illustrated in Figure 10(b). Incorporating XTE in the waypoint navigation algorithm enables the aircraft position to be constantly adjusted.

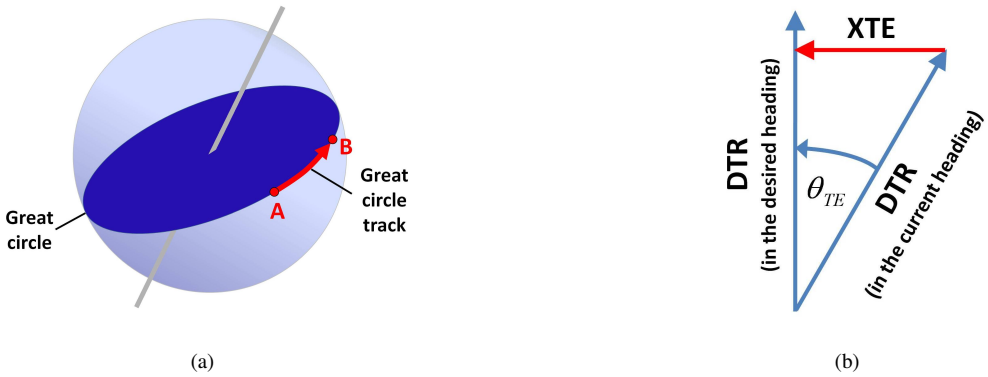

(a) (b)

Fig. 10. Definitions of waypoint navigation components: (a) A great circle track; and (b) Geometric relationship between DTR, θ_{TE} and XTE.

The UAV heading command, ϕ_{cmd}, is calculated as follows:

$$\phi_{cmd} = \phi_T - \theta_{Wc} - B_T + k\theta_{TE} \quad (19)$$

where ϕ_T is the aircraft's true heading, θ_{Wc} is the wind correction angle, B_T is the true bearing to the target, and θ_{TE} is the angle of track error, multiplied by a constant k. In the case of *NavigateWaypoints* function, the value of k is 1.

The bearing/yaw adjustment, along with other parameters calculated by *NavigateWaypoints* are passed to the ACM.

B. Aircraft Control Module (ACM)

The Aircraft Control Module (ACM), details of which are shown in Figure 11, is essentially a collection of displacement autopilots which are used to control the angular orientation of the HEUAV [**?**]. This allows the HEUAV to "fly", i.e. adjust the flight controls (control surface deflections and throttle) so that the desired conditions are met, without human intervention, thus enabling unmanned operations onboard the UAV.

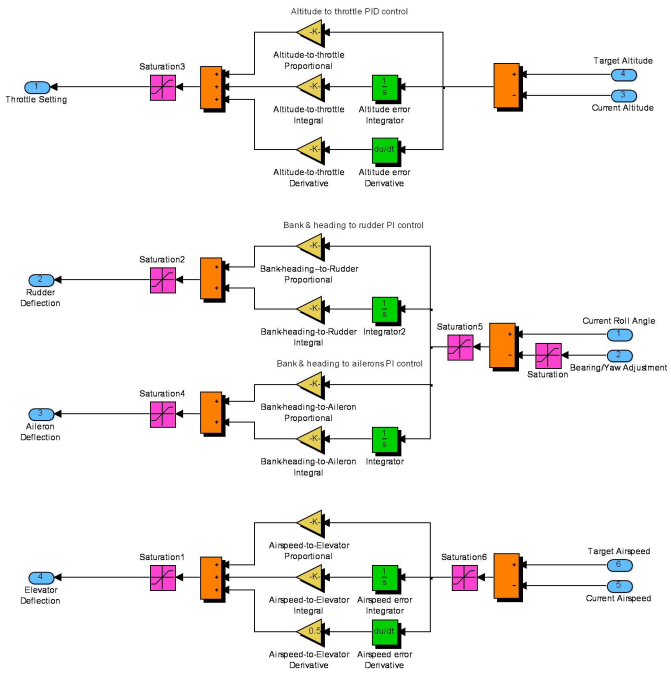

Fig. 11. Aircraft Control Module.

The ***altitude hold control system*** uses a Proportional-Integral-Derivative (PID) controller to maintain the UAV at the desired altitude according to the pre-specified list of waypoints. The inputs to this controller are the *current altitude* and *target altitude*. The difference between the inputs are passed to the PID controller to determine a corresponding value for the *engine throttle* output, ranged between 0.01 (1%) and 1 (100%).

A ***roll attitude autopilot*** is implemented in the ACM with two Proportional-Integral (PI) controllers. This autopilot takes as inputs the *current roll angle* and the *desired bearing/yaw adjustment* as calculated by FPM, and the PI controllers use the difference between these measurements to determine the amount of deflection required for the rudder and the ailerons. The outputs of these PI controllers are the *rudder deflection* and the *aileron deflection* in radians, which are passed to the UAV Block as two of its control inputs.

A PID controller is used in an ***airspeed hold controller*** to maintain the UAV at a constant airspeed of 20m/s (72km/h) when the aircraft is climbing or in cruise, or 30m/s (108km/h) when the aircraft is descending. This change in airspeed command is to ensure that the aircraft would descend at a fast enough rate. The difference between the inputs, *current airspeed* and *target airspeed*, are used by the PID controller to determine the *elevator deflection* in radians, which is the output of the controller.

C. Mission Scenario

As an integral part of the HEUAV simulation process, a baseline mission scenario was constructed. Basic UAV operations such as Climb, Cruise, Descent and Loiter were included in the mission scenario and its flight profile is shown in Figure 12.

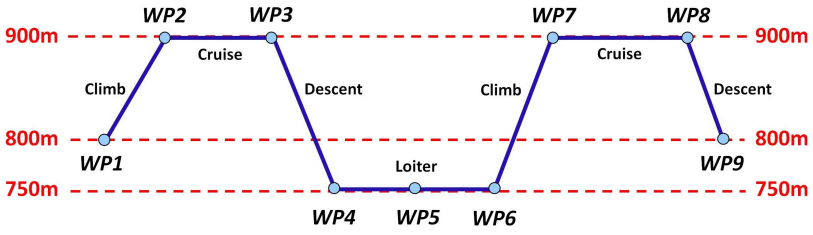

Fig. 12. Flight profile of Mission Scenario 1 (not to scale).

This mission scenario comprises of 100 loops of a series of waypoints, which is entered into the UAVSM in the form of a Waypoint Table and has a distance of approximately 15km per loop. These waypoints are GPS coordinates located in central Queensland, Australia, as illustrated in sequence in Figure 13.

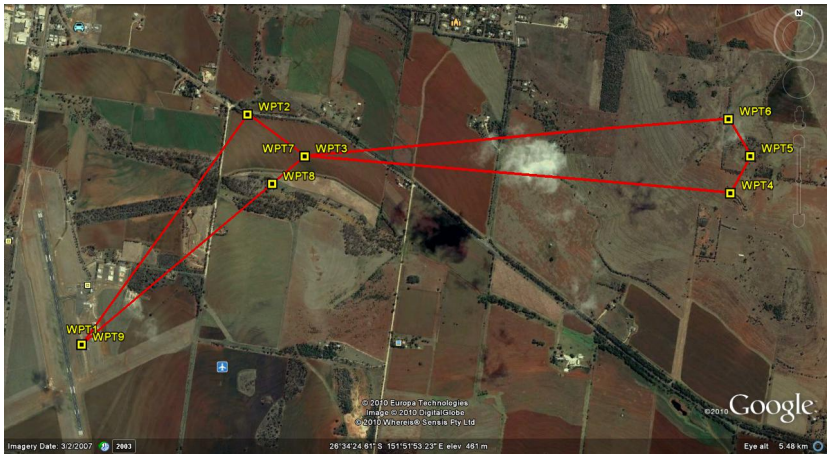

Fig. 13. Mission Scenario 1 with GPS Waypoints in central QLD, Australia (image generated using Google Earth).

It needs to be noted that the in each loop, there is a *loiter* phase, as shown in Figure 12. During this leg, some special mission requirement is carried out, i.e. electric-only flight, video recording, etc.

X. Integrated HEPS Model

Integrating all the components described in §VII and §VIII gives the integrated HEPS model, which is shown in Figure 14.

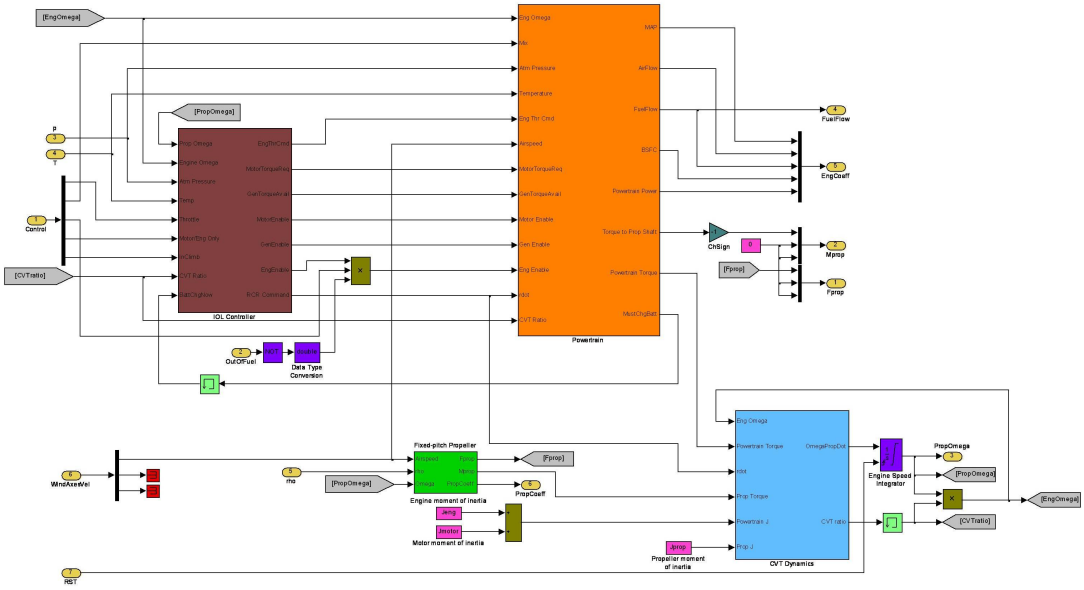

Fig. 14. Inside the integrated HEPS block.

Using this HEPS-integrated model, the mission simulation using the waypoints described in §IX-C was performed. Using the ICE-only and the HEPS model, the results of the simulation are shown in Figures 15 and 16. Figures 17(a) and 17(b) show that the flight path generated by the HEPS-integrated model is a close approximate of that of the ICE-only configuration.

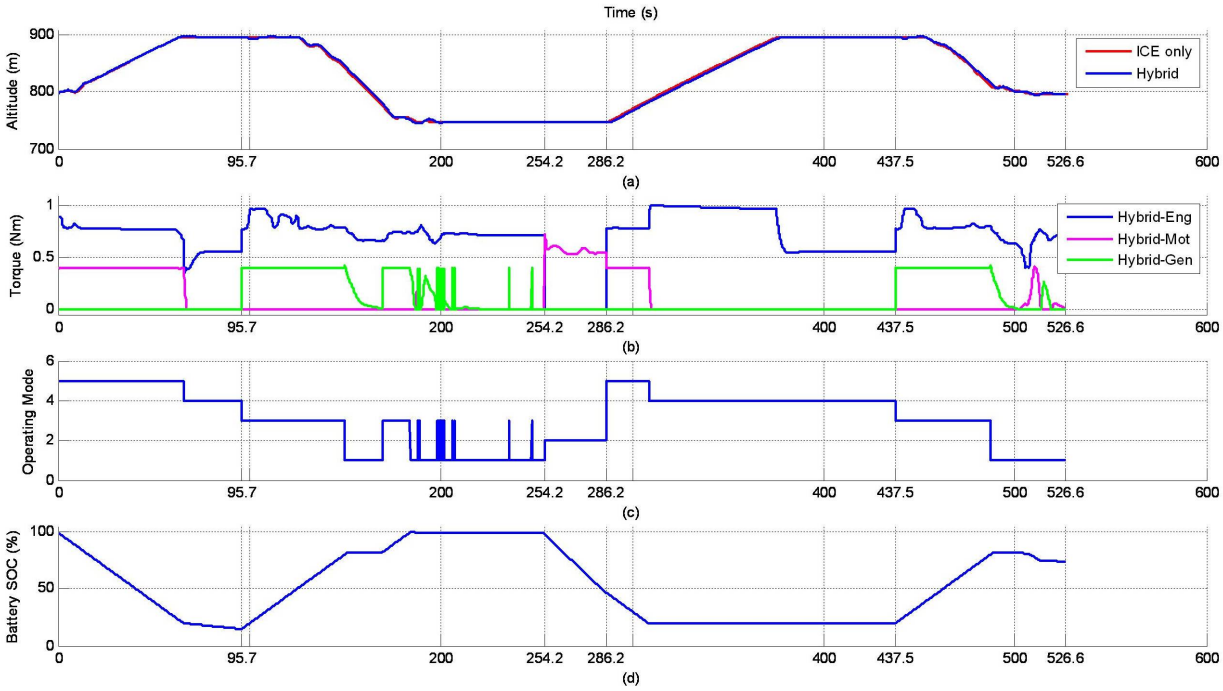

Fig. 15. Data plots of mission simulation using UAVSM with integrated HEPS: (a) Altitude comparisons; (b) Output torque from HEPS components; (c) Operating mode; and (d) Battery SOC.

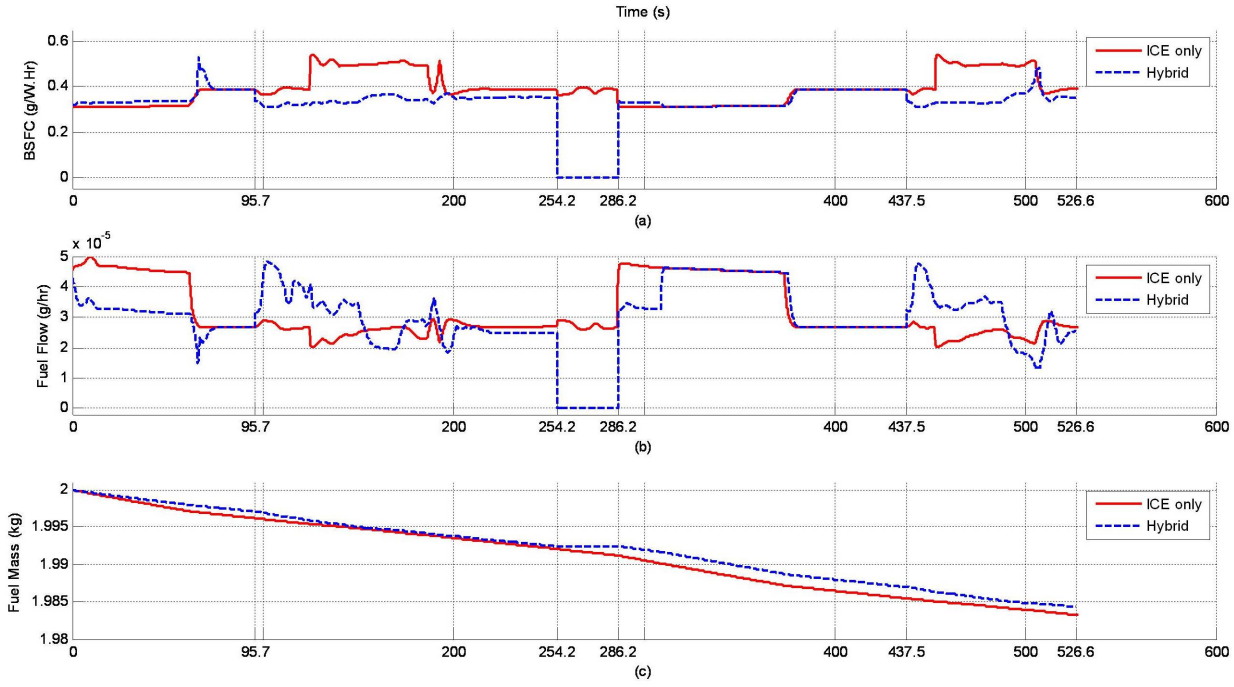

Fig. 16. Simulation data comparisons between using UAVSM with ICE-only and integrated HEPS: (a) BSFC; (b) Fuel flow; and (c) Fuel mass.

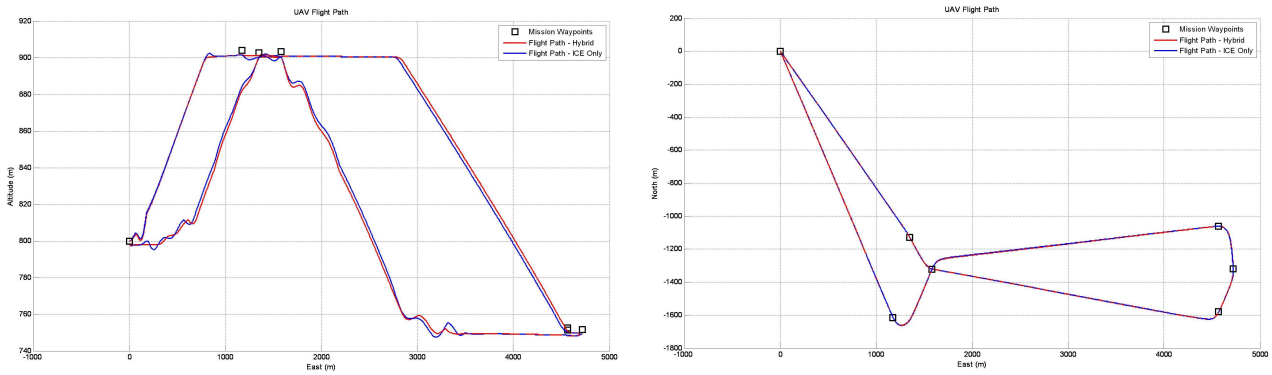

(a) (b)

Fig. 17. Flight path comparison of UAVSM with integrated HEPS and original configuration: (a) Side view; and (b) Top view.

Figure 15(a) shows the altitude profiles of the flight mission using both the original (red) and HE UAVSM (blue), and it can be seen that there is little difference between the two profiles. Figure 15(b) displays the torque outputs of the ICE, EM and Generator components inside the HE UAVSM, which can be seen to correspond to the changing of the operating modes in Figure 15(c). Lastly, Figure 15(d) shows the battery SOC during the simulation, which shows the charging and discharging of the Battery in the duration of the mission as required.

On the other hand, Figure 16 shows the three energy/fuel-related parameters in the simulation, namely BSFC (Figure 16(a)), fuel flow (Figure 16(b)) and fuel mass (Figure 16(c)), for both the original and HE UAVSM. While the BSFC and fuel flow plots are informative as to the instantaneous fuel usage, the fuel mass plot shows the amount of fuel remaining in the tank at any time instance during the simulation. From this plot, it can be seen that there is a visible difference between the fuel used in both configurations.

At the start of the mission ($t = 0s$ to $t = 95.7s$), the UAV was required to climb to an altitude of $900m$. Since the Battery was at full charge (Battery SOC = 100%), this triggered the onset of the "Hybrid Climbing" mode ($OpMode = 5$) and the EM is activated to provide assisting torque to the ICE. The fuel saving effects in this leg is evident in the Fuel Flow plot in Figure 16, which showed a fuel flow of approximately $3 \times 10^{-5} g/hr$ for the Hybrid configuration, compared to approximately $4.5 \times 10^{-5} g/hr$ for the ICE Only configuration. However, the UAV had reached the desired altitude of $900m$ before reaching the desired waypoint coordinates, and since the use of the EM had drained the Battery SOC to below its "Must Charge Now" threshold, the "Engine Only" mode ($OpMode = 4$) was triggered, which minimised the use of the EM and thus the Battery.

The next leg ($t = 95.8s$ to $t = 254.2s$) was a cruise phase, during which the UAV was required to hold an altitude of $900m$, followed by a descent to and hold at $750m$. At the beginning of this leg, the UAV replenished the Battery by entering the "Hybrid Charging" mode ($OpMode = 3$) and the Generator can be seen to receive a constant torque, which charged the Battery. After the Battery SOC had reached the preset threshold of 85%, it was able to return to the "Hybrid Normal" mode ($OpMode = 1$) for most of the remainder of this leg. At $t = 169.7s$, because it was desired that the aircraft enter the "Motor Only" phase with the Battery fully charged, the "Hybrid Charging" mode was once again triggered. This period of enforced charging of the Battery did not last long, as the Battery SOC was at a reasonably high level before this occurred. Therefore, at $t = 184s$, the UAV returned to the "Hybrid Normal" mode, with minor switching to the "Hybrid Charging" mode at moments when the EM, and therefore the Battery, had been activated. In terms of fuel, the "Hybrid Charging" mode required significantly more fuel (between 3×10^{-5} to $5 \times 10^{-5} g/hr$) than the ICE Only configuration (from 2×10^{-5} to $2.5 \times 10^{-5} g/hr$). However, in the "Hybrid Normal" mode, the Hybrid configuration showed smaller fuel flow values than that of the ICE Only configuration.

During the "Motor Only" phase ($t = 254.3s$ to $t = 286.2s$), the UAV entered the "Motor Only" mode ($OpMode = 2$), which used no fuel (zero fuel flow, compared to approximately $2.5 \times 10^{-5} g/hr$ in the ICE Only configuration), but the Battery was drained to a SOC of approximately 50%.

After the "Motor Only" phase, the UAV was in another climbing phase to reach an altitude of $900m$ ($t = 286.3s$ to $t = 437.5s$). At the beginning of this leg, the Battery was adequately charged to power the EM, therefore the "Hybrid Climbing" mode ($OpMode = 5$) was entered. This resulted in a fuel flow of approximately $3.5 \times 10^{-5} g/hr$ for the Hybrid configuration, compared to approximately $4.5 \times 10^{-5} g/hr$ for the ICE Only configuration. However, after approximately $20s$, the lower threshold of the Battery SOC was reached, which prompted the "Must Charge Battery" signal to be activated. This, combined with the fact that the UAV required to climb to a higher altitude, resulted in the UAV operating in the "Engine Only" mode ($OpMode = 4$). During this period of time, the fuel flow for both configurations was identical.

The last leg of the mission ($t = 437.6s$ to $t = 526.6s$) required the UAV to hold at an altitude of $900m$, then descend to the final altitude of $800m$. Initially, the UAV was in the "Hybrid Charging" mode ($OpMode = 3$) because the Battery SOC had reached the lower threshold, and the fuel flow for the Hybrid configuration in this period of time was significantly greater than

that of the ICE Only configuration (between 3.5×10^{-5} to $4.8 \times 10^{-5} g/hr$ versus approximately $2 \times 10^{-5} g/hr$ respectively). But at $t = 487.4s$, the Battery SOC reached the threshold and further charging was not required, the UAV returned to the "Hybrid Normal" mode ($OpMode = 1$). Once again, the Hybrid configuration resulted in a fuel flow smaller in value to that of the ICE Only configuration.

Overall, the fuel consumption for the Hybrid configuration resulted in a saving of $1.09g$, or 6.5%, of fuel. This simulation demonstrated that the implementation of a HEPS on a fixed-wing UAV is capable of reducing the onboard fuel consumption.

XI. Conclusions

This paper presents a review of existing and current developments on the topic of Hybrid-Electric Propulsion Systems (HEPS) for small fixed-wing Unmanned Aerial Vehicles (UAV).

Efficient fuel or energy consumption onboard any aircraft is always crucial in its operations because of the limited weight and space that are available onboard the aircraft. This is even more a problem for small UAVs, therefore it is advantageous to develop methods of further economising the fuel consumption onboard.

The components required in the implementation of a Hybrid-Electric Propulsion System (HEPS) were identified and individually developed. Integration of the Powertrain components – namely Engine, Fuel, Electric Motor, Generator, Battery, CVT Dynamics – was achieved. An IOL analysis on an UAV ICE was performed. Similarly to the Powertrain components, the IOL Controller components – Operating Mode, Power Demand, Engine Operation, Engine Throttle Command, RCR Command and Torque Difference Calculation – were also implemented and integrated. Integration of the IOL Controller and the Powertrain components were successfully carried out, resulting in a HEPS model.

An accurate simulation model of an UAV is required, due to the UAV's multi-physics nature making it impossible to develop an analytical model, to compare the functionalities of the ICE-only and HEPS models. The UAV Simulation Model (UAVSM) was constructed in the MATLAB Simulink environment, utilising the AeroSim Blockset. By integrating the HEPS model into the UAVSM and performing mission simulation, it was demonstrated through simulation that an UAV with the current HEPS configuration was capable of achieving a fuel saving of 6.5%, compared to the ICE-only configuration.

Some aspects of the research conducted here will require further work. These include the following:

- Effects of wind and weather should be investigated and incorporated into the UAVSM;
- The flight mission should be extended to include take-off and landing sequences; and
- Improvements in the implementation of the IOL controller may result in great fuel savings.

References

[1] Unmanned aerial vehicles (UAV). [Online]. Available: http://www.fas.org/irp/program/collect/uav.htm

[2] Jane's unmanned aerial vehicles and targets. [Online]. Available: http://juav.janes.com/public/juav/index.shtml

[3] J. M. Abatti, "Small power: The role of micro and small UAVs in the future," Air Command and Staff College, Air University, Tech. Rep., April 2005.

[4] M. J. Logan, J. Chu, M. A. Motter, D. L. Carter, M. Ol, and C. Zeune, "Small UAV research and evolution in long endurance electric powered vehicles," in *AIAA InfotechAerospace 2007 Conference and Exhibit*, Rohnert Park, CA, USA, 7-10 May, 2007.

[5] R. Glassock, J. Y. Hung, R. A. Walker, and L. Gonzalez, "Design, modelling and measurement of hybrid powerplant for unmanned aerial systems (UAS)," in *5th Australasian Conference on Applied Mechanics*, Brisbane, Australia, 10-12 December, 2007.

[6] A. Bhatia, A. Mendiratta, and M. Vaish, "Comparison of proposed six stroke internal combustion engine with four stroke engine using ideal cycle," in *Proceedings of the 2nd International Conference on Mechanical and Electronics Engineering (ICMEE2010)*, vol. 1, Kyoto, Japan, 1-3 August, 2010, pp. 222–225.

[7] Energy-efficient electric machines. [Online]. Available: http://www.csiro.au/science/ElectricMachines.html

[8] C. Kim, E. NamGoong, S. Lee, T. Kim, and H. Kim, "Fuel economy optimization for parallel hybrid vehicles with CVT," SAE International, Tech. Rep., 1999.

[9] F. G. Harmon, "Neural network control of a parallel hybrid-electric propulsion system for a small unmanned aerial vehicle," Ph.D. Thesis, University of California, Davis, Davis, CA, USA, 2005.

[10] S. B. Wilson, "Micro Air Vehicle Project," *Proceedings of the DARPATech Symposium*, Anaheim, CA, 2002.

[11] L. Petricca, P. Ohlckers and C. Grinde, "Micro- and nano-air vehicles: state of the art," *International Journal of Aerospace Engineering*, vol. 2011, Article ID 214549, 17 pages.

[12] M. Harmats and D. Weihs, "Hybrid-propulsion high altitude long-endurance remotely piloted vehicle," *Journal of Aircraft*, vol. 36, no. 2, pp.321-331, 1999.

[13] World's first serial hybrid electric aircraft to fly at Le Bourget. [Online]. Available: http://www.siemens.com/press/pool/de/pressemitteilungen/2011/corporate_communication/AXX20110666e.pdf

[14] K. Aoki, S. Kuroda, S. Kajiwara, H. Sato, and Y. Yamamoto, "Development of Integrated Motor Assist Hybrid System: Development of the 'Insight', a personal hybrid coupe," SAE International, Tech. Rep., 2000.

[15] A. B. Francisco, "Implementation of an ideal operating line control strategy for hybrid electric vehicles," M.Sc. Thesis, University of California, Davis, Davis, CA, USA, 2002.

[16] K. T. Chau and Y. S. Wong, "Overview of power management in hybrid electric vehicles," *Energy Conversion and Management*, vol. 43, no. 15, pp. 1953–1968, 2002.

[17] F. G. Harmon, A. A. Frank and J.-J. Chattot, "Conceptual design and simulation of a small hybrid-electric unmanned aerial vehicle," *Journal of Aircraft*, vol. 43, no. 5, September-October 2006.

[18] Hyperion, the hybrid propulsion BWB-UAS. [Online]. Available: http://www.uasvision.com/wp-content/uploads/2011/03/Hyperion.pdf

[19] J. Koster, "Hybrid Electric Integrated Optimized System (HELIOS) – design of a hybrid propulsion system for aircraft," in *49th Aerospace Sciences Meeting Including the New Horizons Forum and Aerospace Exposition*, Orlando, FL, 4-7 January 2011.

[20] SOLSTICE: Standalone-electric Optimized Lifting System; Transitional Internal Combustion Engine. [Online]. Available: http://aeroprojects.colorado.edu/10_11/solstice/

[21] J. Paur, "Hybrid power comes to aviation". [Online]. Available: http://ww.wired.com/autopia/2009/07/hybrid-aviation

[22] Modeling and simulation of hybrid electric vehicle (HEV). [Online]. Available: http://www.mathworks.com/mason/tag/proxy.html?dataid=12113&fileid=57988&product=PS&ei=cUOeTPTXK4WsvgOvs5CtDQ&usg=AFQjCNFvo87b0FSb703CwlcZ-M5TxLbI1Q

[23] MATLAB R2011a Documentation - SimDriveline Version 1: Planetary Gear. [Online]. Available: http://www.mathworks.com/help/toolbox/physmod/drive/planetarygear.html

[24] C. M. Greiser, "Implementation of a rule-based open-loop control strategy for a hybrid-electric propulsion system on a small RPA," Masters Thesis, Air Force Institute of Technology, Wright-Patterson Air Force Base, OH, USA, 2011.

[25] P. Singh, C. Fennie, and D. E. Reisner, "Logical progression," in *Electric and Hybrid Vehicle Technology*, 2000, pp. 72-74.

[26] S. Alptekin, D. Deturris, and J. Ervin, "Optimization of the fuzzy logic controller for an autonomous UAV," 2005.

[27] L. Doitsidis, K. P. Valavanis, N. C. Tsourveloudis and M. Kontitsis, "A framework for fuzzy logic based UAV navigation and control," in *2004 IEEE International Conference on Robotics and Automation (ICRA '04)*, New Orleans, LA, USA, 26 April-1 May, 2004.

[28] S. Kurnaz, O. Cetin and O. Kaynak, "Fuzzy logic based approach to design of flight control and navigation tasks for autonomous unmanned aerial vehicles," *Journal of Intelligent & Robotic Systems*, vol. 54, no. 1-3, pp. 229-244, 2009.

[29] M. Salman, N. J. Shouten, and N. A. Kheir, "Control strategies for parallel hybrid vehicles," in *American Control Conference*, Chicago, 2000.

[30] L. Karunarathne, J. T. Economou and K. Knowles, "Fuzzy logic control strategy for fuel cell/battery aerospace propulsion system," in *2008 IEEE Vehicle Power and Propulsion Conference (VPPC '08)*, Harbin, China, 3-5 September, 2008.

[31] L. Karunarathne, J. T. Economou and K. Knowles, "Adaptive neuro fuzzy inference system-based intelligent power management strategies for fuel cell/battery driven unmanned electrical aerial vehicle," *Proceedings of the Institution of Mechanical Engineers, Part G: Journal of Aerospace Engineering*, vol. 224, pp. 77-88, 2010.

[32] Q. Ren, D. A. Crolla, A. Wheatley, "Power management and control strategies for a hybrid vehicle with a dual mode power split transmission," in *5th IFAC Symposium on Advances in Automotive Control*, Pajaro Dunes, CA, USA, 20-22 August, 2007.

[33] A. A. Frank, "Engine optimization concepts for CVT-hybrid systems to obtain the best performance and fuel efficiency," in *2004 International Continuously Variable and Hybrid Transmission Congress*, Davis, CA, USA, 23-25 September, 2004.

[34] B. Cho, "Control of a hybrid electric vehicle with predictive journey estimation," Ph.D. Thesis, Cranfield University, Cranfield, UK, 2008.

[35] M. F. Oudijk, "Optimization of CVT control: For hybrid and conventional drive lines," Masters Thesis, Eindhoven University of Technology; University of California, Davis, Eindhoven, The Netherlands; Davis, CA, USA, 2005.

[36] "AeroSim Blockset, aeronautical simulation blockset, ver. 1.2," 2005.

[37] *Battery*, ser. MATLAB 7.5 Documentation. The MathWorks, Inc.

[38] Air Thunder 5000mAh 6-cell lithium-polymer (Li-Po) battery pack. [Online]. Available: http://www.airthunder.com

[39] A. E. Dortland, "Building a dynamometer test-stand," Eindhoven, The Netherlands: Eindhoven University of Technology; Davis, CA, USA: University of California, Davis, Masters Internship Report DCT-2007-134, 22 October 2007.

[40] C. Brockbank and D. Burtt, "Developments in full-toroidal traction drive infinitely and continuously variable transmissions," in *14th Asia Pacific Automotive Engineering Conference (APAC-14)*, Los Angeles, CA, USA, 5-8 August, 2007.

[41] W. Kriegler, A. Zrim, and G.-J. van Spijk, "IC-Engines and CVTs in passenger cars: A system integration approach," in *IMechE International Seminar S540: Advanced Vehicle Transmissions and Powertrain Management*, London, UK, 25-26 September, 1997.